University College London

Electronic and Atomistic Properties of Palladium Hydride

Thesis submitted for the degree of Doctor of Engineering (EngD)

By

Kay Rigby

Supervisor:

Professor Nora H. de Leeuw

University College London

Department of Chemistry

1st December 2016

Declaration

I, Kay Rigby, confirm that the work presented in this thesis is my own. Where information has been derived from other sources, I confirm that this has been properly indicated and fully acknowledged in the thesis.

Kay Rigby

1st December 2016

Abstract

Palladium hydride is an important material for hydrogen storage, as it can absorb hydrogen at room temperature. Palladium tritide, where tritium is a heavy radioactive isotope of hydrogen, is also of interest because the material has been found to safely store tritium for long periods of time compared with other materials. Due to the radioactive nature of tritium, palladium tritide is an ideal candidate for computational research, allowing parallels between palladium hydride and palladium tritide to be drawn.

A variety of computational techniques have been used in this thesis to undertake a review of the electronic and structural properties of palladium hydride and palladium tritide.

Density Functional Theory has been used to investigate the different possible configurations of non-stoichiometric palladium hydride, when hydrogen vacancies are introduced into the material. The interaction between tritium and its decay product helium-3 has also been studied, as well as helium migration and activation energy.

Two sets of interatomic Buckingham potentials were derived in this work to describe stoichiometric and non-stoichiometric palladium hydride. From these potentials, {100}, {101} and {111} surfaces of stoichiometric and non-stoichiometric palladium hydride were constructed.

Finally, a grain boundary of stoichiometric palladium hydride was constructed using stepped surfaces. Molecular Dynamics simulations were then performed on the grain boundary. The interaction between the grain boundary and water molecules was also investigated.

Acknowledgments

I would like to thank my supervisor Professor Nora de Leeuw for all of her support and encouragement in the past four years. I would also like to thank Dr. Ricardo Grau-Crespo for supporting me with my work and Professor Richard Catlow for his invaluable guidance. I am incredibly grateful to the Atomic Weapons Establishment (AWE) for providing this research topic, as well as funding, and allowing me to conduct my research without constraint.

I would also like to give my thanks to all of the members of the de Leeuw research group past and present and the Molecular Modelling and Materials Science group.

I would particularly like to thank my friends and family for their encouragement over the past four years, in particular my mum and sisters. A special note of thanks goes to Ashley who has always been a huge support both in research and life and to Avone who has always been there for me, especially during the stressful times.

I would like to dedicate this thesis to my dad, whom I am sure would be very proud of me.

List of Publications

The work within this thesis has been discussed in the following publications

and presentations:

Rigby, K., Grau-Crespo, R. de Leeuw, N. H. (2013). "Density functional theory study of the structural and thermodynamical properties of hydrogen vacancies in $PdH_{0.7}$." Abstracts of Papers of the American Chemical Society **246**.

Das, N. K., Rigby, K. and de Leeuw, N. H. (2014). "The effect of helium nano-bubbles on the structures stability and electronic properties of palladium tritides: a density functional theory study." Proceedings of the Royal Society a-Mathematical Physical and Engineering Sciences **470**(2171).

Presentation – Molecular Modelling and Materials Science Centre for Doctoral Training (M3S CDT) Annual Industry Day, July 2014 and July 2010

Conference presentation – American Chemical Society (ACS) National Conference: Chemistry in Motion, September 2013

Poster presentation – AWE Materials Science Research Division (MSRD) Research Exhibition, May 2012

Presentation – AWE Students Conference, Chief Scientists Group, November 2011

Table of Contents

Table of Figures

Table of Tables

Chapter 1

Introduction

This research will investigate the properties of palladium hydride (and isotopes deuteride and tritide), including bulk, surfaces and grain boundaries. It aims to expand on the existing literature, as well as further proving that palladium is an effective hydrogen storage material. This will be completed using a variety of computational techniques including density functional theory, interatomic potential derivation and classical molecular dynamics.

Palladium has been selected for research as it has a significantly longer tritium storage lifetime before mechanical failure compared with other metal tritides, showing potential for the long-term safe storage of radioactive tritium. Therefore, the structural and electronic properties of palladium, palladium hydride and ultimately palladium tritide should be investigated to determine the mechanism of hydrogen isotope storage and the stability of the surfaces and bulk material.

1.1 Material Properties

Palladium is malleable, ductile and has a face-centred cubic (fcc) structure, as shown in Figure 1-1 where palladium atoms exist at the corners and face-centres of the unit cell.

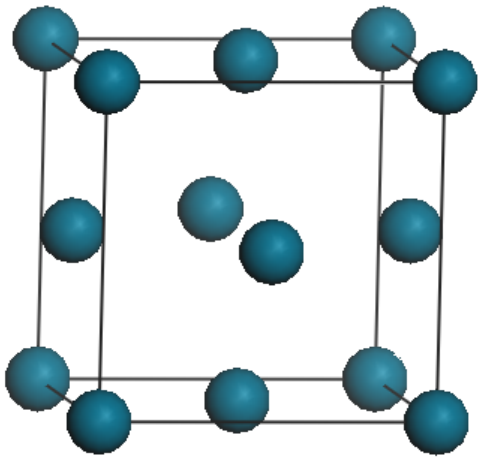

Figure 1-1: The face-centered cubic lattice structure of palladium metal, with palladium atoms in blue.

Palladium has a closed-shell $[Kr]4d^{10}$ electronic structure which allows for a reasonably high helium capacity without the helium reacting with the host metal lattice. Helium to palladium atom ratios of 0.5 have been observed (Abell *et al.* 1990). Palladium is also highly desirable for tritium storage, as it absorbs and desorbs tritium at room temperature (Joubert and Thiebaut 2009), making the process cost effective. However, this means that experimentally a H_2 over-pressure is required to maintain a given hydrogen content within the metal.

The hydrogen atoms sit within the octahedral interstitial sites of the palladium metal, creating a “rock-salt” structure, as shown in Figure 1-2.

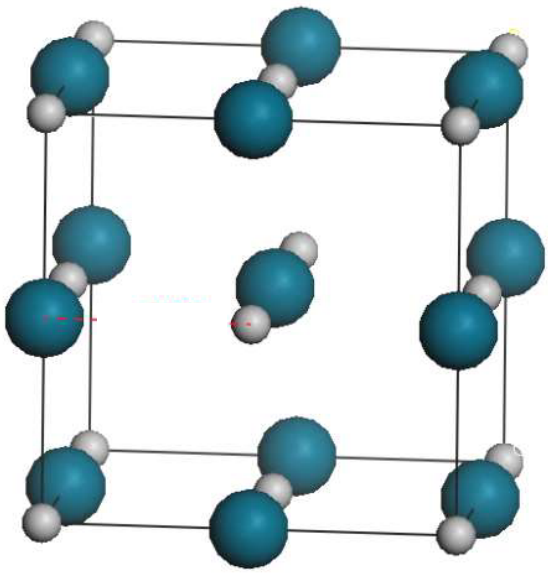

Figure 1-2: The “rock-salt” face centered cubic (fcc) structure of theoretical palladium hydride (PdH), where the palladium atoms are blue and the hydrogen atoms are white.

Most importantly, palladium can safely store tritium for up to 16 years before mechanical failure (Holder and Wermer 1995), with some studies reporting palladium tritide lifetimes of up to 19 years (Zeng et al. 2009). These lifetimes are significantly higher than those found for other metal tritides, which can be as low as 5 years. It is essential for a tritium storage material to allow both the safe insertion and removal of pure tritium without any critical damage being imposed on the storage material.

Tritium is a radioactive, heavy isotope of hydrogen, containing one proton, one electron and three neutrons, with a half-life of 12.32 years (Beavis and Miglioni 1972). The safe storage of tritium is essential for the long-term containment of

harmful radiation. The products of tritium beta-negative decay are as follows, (where v_e is an electron antineutrino):

Equation 1-1: The products of tritium beta-negative decay – helium-3, an electron, an antineutrino and 28.6 keV energy.

$$^{3}_{1}T \rightarrow ^{3}_{2}He + ^{0}_{-1}e^{-} + v_e + 28.6keV$$

Tritium can be produced by: irradiating lithium oxide (Briec et al. 1986); the addition of a neutron to heavy water (D_2O); and the decay of uranium-235 during nuclear fission.

Tritium is primarily stored as a gas in solid metal structures such as $LaNi_5$. Tritium can also be stored in (and extracted from) liquid metals such as lithium, in which it has high solubility (Moriyama et al. 1995). Tritium extraction methods from liquid lithium include: molten salt extraction where liquid lithium is mixed with lithium halides; gettering or trapping using solid yttrium; and fractional distillation of deuterium and tritium (Moriyama et al. 1995). Although liquid lithium may be an advantageous tritium storage material, there are many engineering issues associated with the storage and processing of liquid metals, particularly because of their corrosive properties.

Due to the radioactive nature of tritium, many experimental studies have been conducted on palladium hydride rather than palladium tritide. Parallel conclusions can be drawn between palladium hydride and palladium tritide, as both materials have the same “rock-salt” structure and only slight differences in lattice parameter and equilibration formula; $PdH_{0.7}$ with a lattice parameter

of 4.040 Å (Maeland and Flanagan 1966) and $PdT_{0.67}$ with a lattice parameter of 4.033 Å (Cowgill 2004). Computationally, it is possible to make comparisons between palladium hydride and palladium tritide, as well as studying isotope effects.

1.1.1 Hydrogen Absorption

As tritium is an isotope of hydrogen, it is reasonable to assume that hydrogen absorption into a storage material is a good approximation for a tritium absorption mechanism. Hydrogen absorption is well documented, as hydrogen storage plays an important role in the current search for efficient energy storage. However, isotope effects must be considered when undertaking quantitative studies, where the relatively large atomic weight difference between hydrogen and tritium has a large effect on energetic values. Also, as hydrogen is not radioactive, clearly hydrogen absorption studies do not consider tritium radioactive decay and subsequent evolution of helium within the metal lattice.

Okuyama *et al.* undertook extensive studies on the absorption and migration of hydrogen atoms on the (100) surface of bulk palladium, using thermal desorption spectroscopy (TDS) (Okuyama, Siga et al. 1998). A simple model for hydrogen migration was proposed: (1) a hydrogen molecule chemisorbs, resulting in dissociation into hydrogen atoms, onto the Pd (100) surface; (2) the hydrogen atom migrates to occupy an octahedral subsurface site; (3) the hydrogen atom migrates further to a bulk site in the metal. Hydrogen was found to absorb into palladium, after the formation of a complete surface monolayer,

via tetrahedral sites on the surface of the metal and migration depended on only local geometry of the substrate. Tetrahedral sites are found on the Pd (111) surface and hydrogen absorption is facile, whereas the absorption sites on a perfect Pd (100) surface were octahedral, with a high activation energy barrier. At surface temperatures below 120 K, absorbed hydrogen existed only at subsurface sites, whereas a surface temperature above 150 K was required to enable absorbed hydrogen to reach the bulk sites ~10 μm from the metal surface. The high energy required for hydrogen absorption from the surface to subsurface sites was thought to be due to the movement of the first and second layer of palladium atoms, as the hydrogen atom passed through the layers before coming to rest in an octahedral subsurface site.

Zhu *et al.* studied the mechanism of hydrogen absorption by palladium powder as shown in Figure 1-3 where the α-phase is pure palladium and the β-phase is palladium hydride (Zhu et al. 2008). The reaction was broken down into the following steps; (1) physisorption of hydrogen molecules; (2) dissociation of hydrogen molecules and chemisorption; (3) surface penetration by hydrogen atoms; (4) diffusion of hydrogen atoms through the hydride layer, either by an interstitial or vacancy mechanism; (5) hydride formation at the metal/hydride interface.

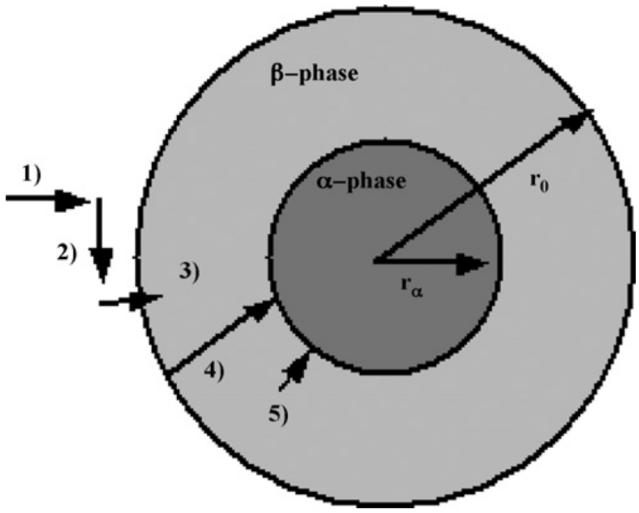

Figure 1-3: Diagram to show the different stages of hydrogen absorption in a palladium powder particle where the α-phase is pure palladium and the β-phase is palladium hydride. (1) physisorption of hydrogen molecules; (2) dissociation of hydrogen molecules and chemisorption; (3) surface penetration by hydrogen atoms; (4) diffusion of hydrogen atoms through the hydride layer, either by an interstitial or vacancy mechanism; (5) hydride formation at the metal/hydride interface. ***(Zhu et al. 2008)***

Ruda *et al.* compared hydrogen absorption in 1 nm and 2 nm palladium nanoparticles and bulk palladium by computationally calculating pressure-composition isotherms (Ruda et al. 2010). It was found that the isotherms calculated for the bulk system were comparable with experimental data. Pressure-composition isotherms calculated for nanoparticle systems with a radius of 2 nm or larger showed completely different slopes than those for the bulk system, suggesting a difference in hydrogen absorption mechanism. However, the isotherm for the 1 nm nanoparticle system showed a distinctive

plateau, similar to that seen for the bulk system. All calculated isotherms for the nanoparticle systems were different from those obtained experimentally, which was attributed to the fact that nanoparticle grains cannot be isolated experimentally but were isolated in the computational studies. Radial distributions of hydrogen in a 1 nm nanoparticle at different concentrations (H/M = 0.76 and H/M = 0.35) showed that hydrogen atoms existed in the subsurface region of the nanoparticle. Evidence for this is shown particularly for the lower hydrogen concentration studied, where the majority of hydrogen atoms existed within the outer 0.2 nm of the nanoparticle.

1.1.2 Hydrogen Desorption

Ease of tritium desorption from the storage material must also be considered, if pure tritium is to be extracted for use in other applications, such as nuclear fusion.

Okuyama *et al.* studied desorption of hydrogen atoms from a palladium metal surface, with an adsorbed deuterium surface monolayer (Okuyama, Siga et al. 1998). Little deuterium was detected, using Thermal Desorption Spectroscopy (TDS) to analyse the composition of the desorbed species, suggesting that desorption from within the metal occurred without inducing any significant disturbance to the adsorbed surface monolayer.

The U.S. Department of Energy extracts tritium for use in nuclear weapons from tritium producing burnable absorber rods (TPBARs) which are a waste product of nuclear fission reactors (Clark 2004). Previous methods of tritium extraction employed by the U.S. Department of Energy include the use of

heavy water reactors and dismantled nuclear weapons. During nuclear fission, lithium-6 is irradiated by neutrons, producing tritium gas which is trapped in solid zirconium within the TPBAR. The tritium is later extracted for future use. Studies conducted by the U.S. Department of Energy show that containment of used TPBARs, with residual tritium present, is effective for up to 24 years with an internal temperature of approximately 350 K (Clark 2004).

1.1.3 Phases of Palladium Hydride

The phase diagram of palladium hydride consists of three regions (Figure 1-4) (Flanagan and Oates 1991), a low hydrogen concentration (α-phase) where $\alpha_{max} = PdH_{0.015}$, a high hydrogen concentration (β-phase) where $\beta_{min} = PdH_{0.607}$ and an intermediate α+β-phase (Adams and Chen 2011). During the β-phase, the palladium lattice expands in order to allow for increased tritium capacity at octahedral sites. Despite each region being classed as a “phase” and having vastly different hydrogen concentrations, no overall change in the microstructure is observed. The α+β-phase is otherwise known as the miscibility gap and the maximum temperature at which this phase occurs, the critical temperature, is 566 K (Joubert and Thiebaut 2009). Above this temperature, a transition directly from α-phase to β-phase occurs.

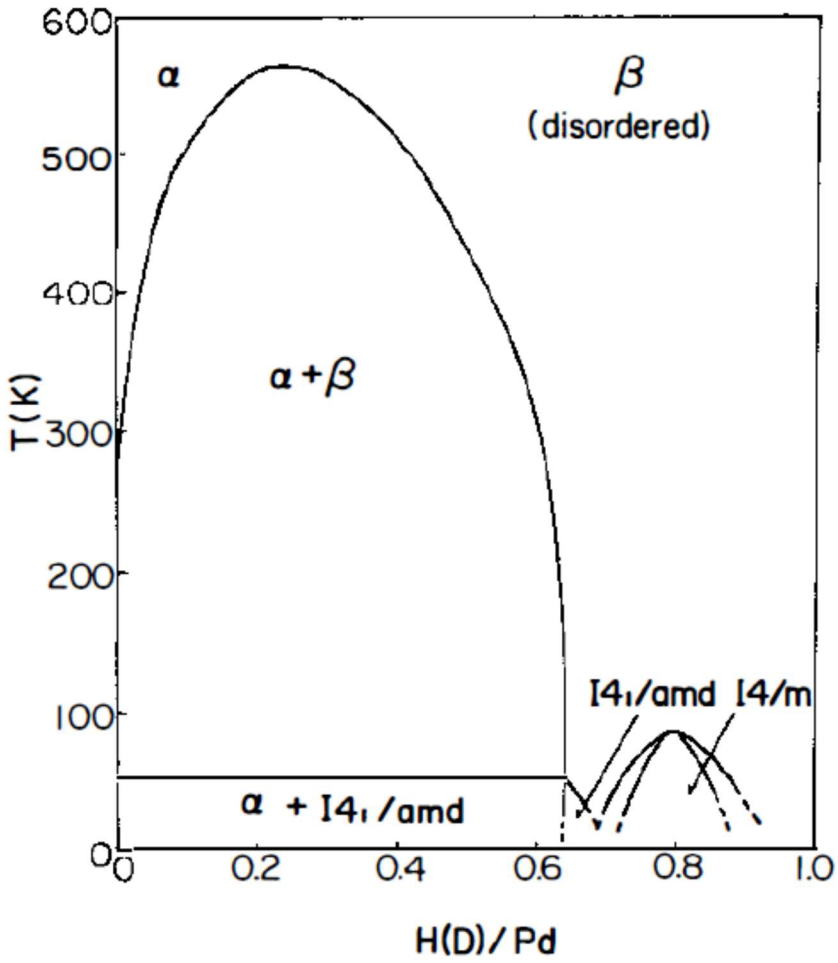

Figure 1-4: The phase diagram of palladium hydride, including low hydrogen concentration (α-phase) where $\alpha_{max} = PdH_{0.015}$, high hydrogen concentration (β-phase) where $\beta_{min} = PdH_{0.607}$ and an intermediate miscibility gap (α+β-phase). (Flanagan and Oates 1991)

The structure of palladium hydride has been well reported for several decades. It has been found that hydrogen atoms within palladium hydride are most stable in the octahedral interstitial sites of palladium metal (Worsham et al. 1957). Octahedral interstitial sites have a larger free volume than tetrahedral interstitial sites, as shown in Figure 1-5 (Zu et al. 2009). Zu et al. observed that the formation energy of a helium atom in an octahedral interstitial site of palladium was 0.12 eV lower than that of a tetrahedral interstitial site. This

implies that the hydrogen atoms situated in octahedral sites will induce less destabilizing strain on the metal lattice than those found in tetrahedral sites. The close proximity of a tetrahedral interstitial hydrogen atom to the palladium metal atoms may cause deformation of the lattice structure. Studies on the binding energy of a hydrogen atom to octahedral and tetrahedral interstitial sites, show a significantly larger binding energy for tetrahedral sites, meaning that the hydrogen atom is more weakly bound (Kamakoti and Sholl 2003).

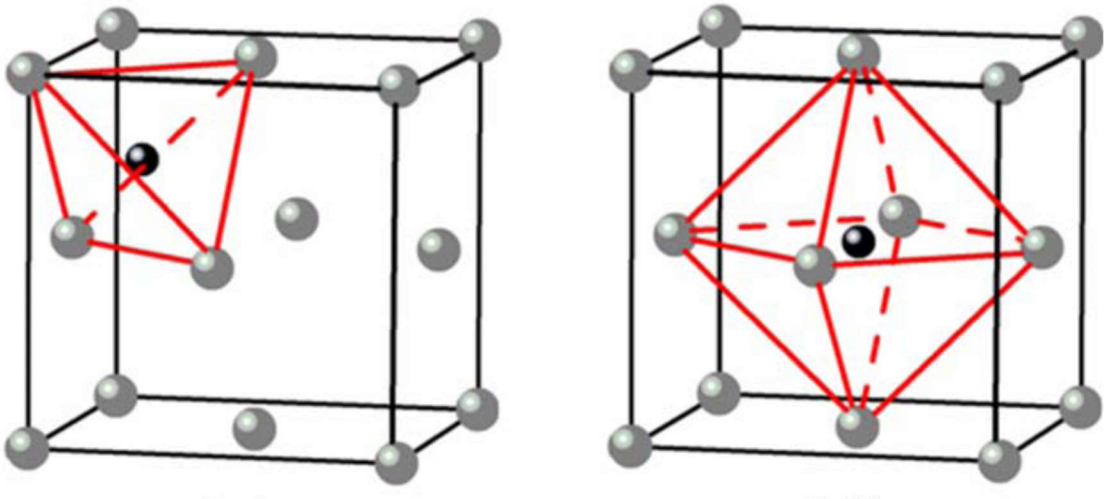

Figure 1-5 - A comparison of the free volume of tetrahedral (left) and octahedral (right) interstitial sites occupied by a tritium atom in a face centered cubic lattice of palladium metal. (Zu et al. 2009)

Slight lattice expansion occurs from pure palladium metal (3.890 Å) to α-phase palladium hydride (3.894 Å), however a larger lattice expansion occurs in the transition from α to α+β-phase palladium hydride (4.040 Å) (Flanagan and Oates 1991). In Figure 1-6, (a) shows hydrogen absorption and diffusion occurring in α-phase palladium hydride, which can be considered as a solid solution of hydrogen. As hydrogen content increases, interactions between hydrogen atoms leads to a stabilised hydride structure (b) (Berube et al. 2007).

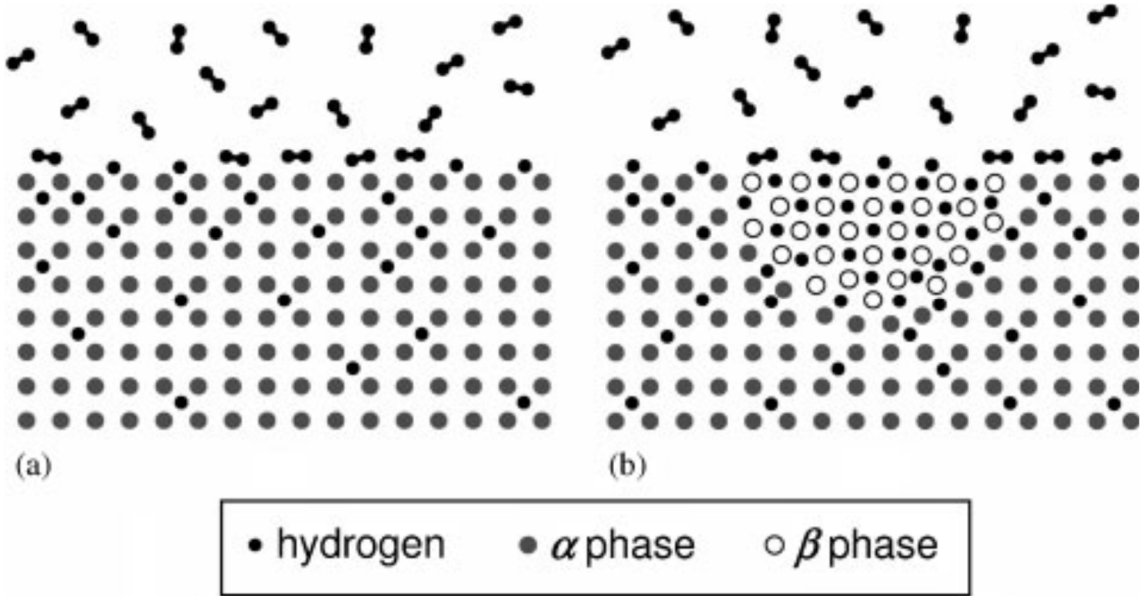

Figure 1-6: Hydrogen absorption and diffusion within palladium hydride. Where (a) shows α-phase palladium hydride, which can be considered as a solid solution of hydrogen and (b) shows increased hydrogen content and a stabilised hydride structure. (Berube et al. 2007)

The pressure-composition isotherm (Figure 1-7) of PdH shows three distinct regions, with the inflection points of each isotherm representing a phase transition (Joubert and Thiebaut 2009). The low concentration α-phase occurs at extremely low pressures, before a rapid increase in hydrogen content (α+β-phase), shown as a plateaux in Figure 1-7. Finally, at higher pressures, the increase in hydrogen concentration slows, representing a β-phase composition.

At ambient temperatures and pressures, the maximum H/Pd ratio is found to be 0.7, determined from pressure-composition isotherms. This suggests that ~ 30% of the octahedral interstitial sites in $PdH_{0.7}$ are unoccupied and can be thought of as hydrogen vacancies. The abundance of hydrogen vacancies in palladium allows for facile hydrogen diffusion within the metal. It is not clear

from the literature as to why stoichiometric PdH is only achieved at extremely high pressures.

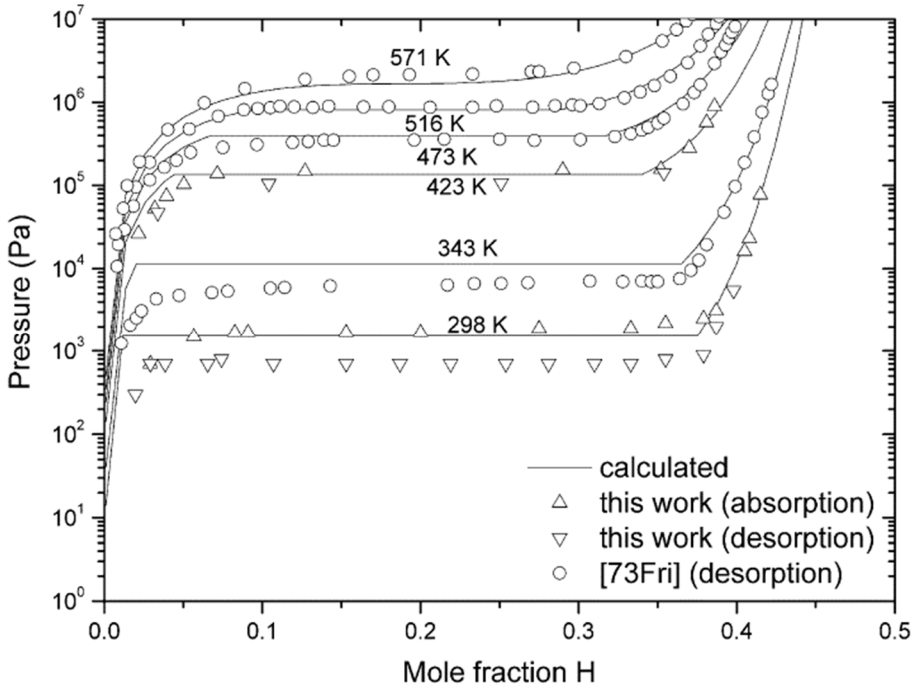

Figure 1-7: Pressure-composition isotherms of palladium hydride at a range of temperatures, where the inflection points indicate phase transitions between α-phase, α+β-phase and β-phase palladium hydride. (Joubert and Thiebaut 2009)

A hydrogen atom diffuses through the metal lattice via a series of thermally induced “hops”. Intuitively, the diffusion path of a hydrogen atom between two octahedral interstitial sites can be thought of as; octahedral – tetrahedral – octahedral, as this is the shortest diffusion length. This diffusion pathway is found to be the most favourable path for the hydrogen atom (Gillan 1986), with the diffusion activation energy (0.24 eV) being approximately equal to the difference in energy between a tetrahedral and octahedral interstitial hydrogen atom.

If all octahedral interstitial sites are occupied by hydrogen atoms, the resulting hydride formula is PdH (i.e. a 1:1 ratio). This formula is incredibly difficult to attain but has been achieved by ion implantation at liquid helium temperatures of between 9 and 11 K (Stritzke and Buckel 1972). Additionally, H/ Pd ratios > 1 can be achieved by electrolysis or low temperature ion implantation. For example, supersaturated palladium deuteride with the formula $PdD_{1.4}$ was achieved through ion implantation below 100 K, however above 120 K the concentration of deuterium decreased significantly (Myers et al. 1991). However, ion implantation can severely damage the structural integrity of palladium, leading to mechanical failure. Several studies of PdH_x where $x > 1$ have been undertaken, leading to observations of palladium vacancies under extremely high pressures and temperatures (Fukai and Okuma 1994).

As palladium is a rare metal, experimental and subsequently large-scale industrial use can be expensive. Therefore it is useful to investigate materials with a lower palladium content or alternative metal tritides as potential tritium storage materials. Research has focused on the behaviour of materials such as powders, palladium alloys and other metal tritides.

Nanoporous metal tritides enable helium molecules to diffuse through pores in the material to the surface, theoretically preventing accelerated release and subsequent rupture of the storage material. Robinson *et al.* synthesised palladium and platinum powders which were stable up to 150°C, containing particles of 50 nm in size with 2-3 nm nanopores throughout (Robinson et al. 2009). Metal particles were grown on close packed cylindrical templates

composed of a surfactant, oligo(ethylene oxide) hexadecyl ether. The template was washed away to leave the nanoporous metal. This process was shown to be scalable, with the production of gram-scale quantities of the powder. Future research by this group will focus on introducing hydrogen into the nanoporous structure (Robinson et al. 2009).

By utilising the properties of certain metals, alloys with palladium can be formed to enhance tritium storage capacity, mechanical strength and microstructure.

Thiebaut *et al.* researched the changes in structure of Pd-Rh and Pd-Pt alloys during tritium decay within the solid lattice (Thiebaut et al. 1998). It is interesting to study these alloys, as platinum is in the same period as palladium and rhodium has a similar atomic weight to palladium. The individual metals in the alloys were found to be well distributed throughout the material and did not form clusters. Both Pd and Rh absorbed tritium readily, whereas Pt was a poorer tritium absorbent. Therefore a larger tritide content was found within the Pd-Rh alloy than the Pd-Pt alloy. The Pd-Pt alloy exhibited isolated finite sized defects of helium close to Pt atoms, as Pt repels tritium, leaving more space nearby for helium cluster formation. Pt also has good elastic properties, which was indicated by significant lattice swelling within the Pd-Pt material. Conversely, Rh had little effect on the structure of the Pd-Rh material over time.

Holder and Wermer studied tritium loading and thermodynamic properties of Pd-Ni and Pd-Co alloy tritides, with two different compositions of 2.8 and 5.2

wt. % of Ni or Co (Holder and Wermer 1995). Nickel is in the same period as palladium and also exhibits a face-centred cubic structure. Alloys with a higher nickel or cobalt content were harder to activate and tritium loading was slower than the lower wt. % alloys, although cobalt alloys were easier to load than nickel alloys. Enthalpy change (ΔH) values were higher in the 2.8 wt. % alloys compared to the 5.2 wt. % alloys and were comparable to values for pure palladium, showing that as the alloy content increased, ΔH decreased. It should be noted that all ΔH values were positive, where ΔH (pure Pd) = 16.6 kJ mol^{-1} T^{-1}, ΔH (2.8 wt. %) = 15.8 to 16.2 kJ mol^{-1} T^{-1} and ΔH (5.2 wt. %) = 13.6 kJ mol^{-1} T^{-1}. It was also shown that plateau pressures increased as the wt. % of the alloy increased. However, a higher plateau pressure was thought to lead to a lower tritium capacity. Therefore, when selecting a suitable alloy content there must be a compromise between lower ΔH, and therefore a more stable tritide, and increased tritium capacity of the metal. The entropic change (ΔS) was found to be similar for all alloys but was higher in alloys compared to pure palladium, due to increased disorder found for a material containing two different metals compared to a purely elemental material.

1.2 Other Metal Tritides

Thiebaut *et al.* compared helium retention and ageing effects in palladium and $LaNi_5$ tritides (Thiebau et al. 2007). It was found that both tritides retained at least 95% helium for up to 9 years. However, the thermodynamic properties of $LaNi_5$ were lost after 1.8 years and structural properties lost after only 2.8 years. Early structural failure was caused by helium atoms mainly binding to small tetrahedral interstitial sites within the bulk material, leading to significant

lattice distortion and swelling. Palladium tritide was found to retain structural properties for at least 10 years, due to the rapid formation of 1.5 nm helium bubbles within the first 8 months of tritium ageing. The bubbles existed as local defects with a finite volume and left the interstitial sites free, having little effect on the structure and subsequent swelling of the lattice. Thiebaut *et al.* suggested that $LaNi_5$ could be used for short term tritium storage only, otherwise the material would have to be replaced regularly, presenting issues of waste management (Thiebaut et al. 2007). It was found that palladium is much more suitable than $LaNi_5$ for long term tritium storage, however palladium is a rare metal and therefore expensive, incurring high start-up costs.

Beavis and Miglioni compared the effects of tritium decay and subsequent helium release within five different metal films; erbium, holmium, scandium, titanium and yttrium (Beavis and Miglioni 1972). All of the metal tritides showed mechanical failure within the first five years after tritiding, compared with palladium tritide, which has a lifetime of up to 19 years (Emig et al. 1992). Scandium ditritide presented a higher initial expansion rate than other tritides. All of the metals studied showed stepped crater formation over time due to the aggregation and eventual blistering of helium bubbles. Each tritide also exhibited enhanced structural failure at weak points within the metal, such as scratches on the film surface.

Nickel is in the same period as palladium in the periodic table and also has a face centered cubic structure; therefore it is interesting to investigate whether

nickel and palladium have similar properties regarding tritium storage and helium bubble evolution.

Nickel metal hydrides have been extensively researched and are a suitable material for use in batteries for electric vehicles. Desirable properties include high energy density, high power density and a large number of charge-discharge cycles before mechanical failure (Ovshinsky et al. 1993).

Orimo and Fujii (Orimo and Fujii 2001) synthesised Mg/Ni hydrides in order to improve the hydriding of magnesium, as seen for Pd/Mg alloys. The use of nickel rather than palladium was attributed to the higher % wt. of hydrogen obtained, due to nickel being a lighter, 3d, metal.

Yang *et al.* performed MD simulations to compare the formation energy and helium binding energy of helium-vacancy clusters in nickel and palladium lattices (Yang et al. 2004). In the nickel lattice, the formation energy was found to increase with increasing number of helium atoms in 12 vacancies (He_nV_{12}). However for palladium, formation energy was constant, before increasing when there were more than 12 helium atoms in the 12 vacancies, a He/V ratio of 1. This trend was attributed to the closed-shell electron configurations of palladium and helium. The binding energy of a helium atom to an existing helium-vacancy cluster in nickel decreased as the He/V ratio increased, until a He/V ratio of 5, where the binding energy began to increase. The increase in binding energy was thought to have been caused by atom displacement, also seen by Liu *et al.* where the large, high pressure helium cluster pushes a metal atom from its lattice position and a new vacancy is created, therefore

decreasing the He/V ratio (Liu et al. 2006). No increase in binding energy was found for palladium up to a He/V ratio of 7, as the binding energy initially decreased before becoming a constant energy at approximately 1.5 eV. Therefore it can be concluded that palladium has a much larger helium capacity than nickel, as no metal atom displacement was found for palladium.

1.3 Helium-3

The helium-3 generated by tritium beta-negative decay, as shown in Equation 1-1, has a closed-shell $1s^2$ electron configuration, meaning that it is chemically unreactive towards other species and thus is highly insoluble in metals. Helium can be inserted into metals via atom bombardment or ion implantation, however these processes may damage the storage material. Therefore, helium-3 produced from tritium beta decay within a metal is the most viable method for studying the behaviour of helium in metals, as the storage material is left relatively undamaged at low helium concentrations. The closed-shell electronic configuration of helium-3 also allows for the efficient removal of pure tritium from a storage medium, upon heating, without removing any undesired helium.

Helium is usually insoluble in metals, meaning that studying the generation of helium within metal tritides is important for investigating microscopic and macroscopic, particularly structural, changes to a metal lattice caused by the presence of helium. Due to the low solubility of helium within metals (Lasser 1987), problems can arise with the direct injection or ion implantation of helium

atoms into metal structures. The two most viable mechanisms for the introduction of helium into metals are discussed in the following sub-sections.

Several experimental methods for helium injection into metals exist and pose a realistic alternative to the hazardous handling of tritium. Ion injection can provide a high helium concentration and also accurate helium concentration control within the metal lattice (Stritzke and Buckel 1972). However, improvements to existing methods are required to minimise microscopic damage to metal lattices during ion injection.

Zheng *et al.* implanted helium into titanium and titanium alloy films using magnetron sputtering deposition (Zheng et al. 2005). A mixed stream of ionised helium and argon gas was fired at a target, causing helium and argon atoms with decreased energy to backscatter into the titanium film. Scanning electron microscope (SEM) images showed that 2-5 nm helium bubbles aggregated at grain boundaries and dislocations in the titanium film. The optimum He/Ti ratio was found to be approximately 0.16, with helium atoms homogenously distributed throughout the bulk of the film. Evidence of helium release from the film upon heating was shown by a decrease in the He/Ti ratio to 0.11 at 923 K.

Magnetron sputtering possesses some advantages as a helium implantation method, such as little damage to the film and deep implantation, with few helium atoms existing at the surface of the film. However, there are several drawbacks to this method; the optimum He/Ti ratio is quite low and the distribution of helium bubbles within the film depends on the location of inherent defects.

The generation of helium during tritium decay has been an important topic of experimental and, more recently, computational research for many years.

The presence of helium in metals as a consequence of tritium decay is the most effective way of implanting helium homogenously throughout the storage material, without causing excessive lattice damage.

Over time, tritium decays within a metal storage material, leading to the gradual production of helium which is trapped deep within the metal for many years. This process is known as tritium ageing and the rate of ageing can depend on the metal storage material (Holder and Wermer 1995) and on helium concentration but is independent of initial metal-tritium stoichiometry (Camp 1977). For example, studies conducted on $TiT_{1.5}$ and $TiT_{1.8}$ found that the critical helium concentration (optimal He/M ratio before macrostructural failure) for both stoichiometries is ~0.3 (Camp 1977).

Research topics on the study of the behaviour of helium in metals range from helium migration, helium bubble formation and nucleation to the creation of defects within the metal lattice. The following sections review each of these mechanisms.

The process of increasing helium concentration leading to helium bubble formation and eventual accelerated release and material rupture is described in Figure 1-8.

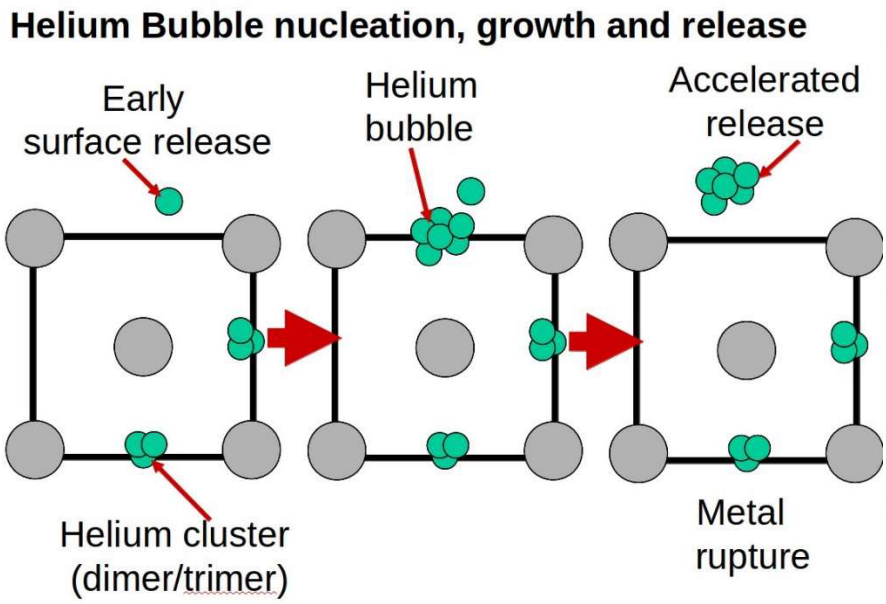

Figure 1-8: Diagram of helium evolution within a palladium tritide lattice. 1) At low helium concentrations, slow helium release occurs through surface cracks and small helium clusters are formed. 2) As helium concentration increases, clusters combine to form larger helium bubbles. 3) At a critical helium concentration, accelerated release occurs and the metal irreversibly ruptures.

Initially when little tritium decay has occurred, initially isolated, immobile helium atoms are randomly distributed in octahedral interstitial sites throughout the metal lattice. As helium concentration increases, small helium clusters made of one of two helium atoms develop and continue to grow. It is also at this time that some helium atoms are released from cracks in the surface of the material. As the material ages, the small helium clusters aggregate to form larger helium bubbles. Once a large enough cluster size is reached, the clusters connect with one another, at a He/M ratio above 0.2. (Beavis and Kass 1977).

At a critical helium concentration, the helium bubbles are rapidly released from the material, in a process called accelerated release, which causes the

material to rupture. This process occurs when the rate of helium release is greater than or equal to the rate of helium generation (Thiebaut et al. 2007). Accelerated release must be prevented or delayed for as long as possible, in order to avoid potentially dangerous tritium leaks into the environment. Therefore, a suitable tritium storage material would need to have a large capacity for helium and the ability to expand and withstand mechanical stress whilst still retaining its overall macrostructure. It is also important to study accelerated release in order to predict when it will occur and therefore draw conclusions on the lifetime of a metal lattice before critical failure. Here, it is important to consider the ratio of helium to metal atoms where, R = He/M. The critical helium concentration, R_c, is found to be between 0.2 and 0.3 for most metals (Abell et al. 1990), which is larger than the He/Ti ratio of 0.16 obtained via helium injection by Zheng *et al. (*Zheng *et al. 2005).* However for palladium metal $R_c = 0.5$, (Abell et al. 1990) showing that palladium has a greater capacity for helium than other metals.

Gupta and Gupta found that as tritium decays, helium is created and exists in a metastable state at octahedral interstitial sites in palladium tritide (Gupta and Gupta 2002). Further evidence for octahedral interstitial helium atoms is presented by Zu *et al.* (Zu et al. 2009) and Zeng *et al* (Zeng et al. 2009). Helium atoms exhibit little diffusion through the metal lattice from their generation site, as they have a low average energy of ~ 1eV (Beavis and Kass 1977).

Xia *et al.* performed a molecular dynamics (MD) study to compare the random interstitial “hopping” of a helium atom in nickel and palladium lattices (Xia et al. 2006). It was found that the helium atom began to “hop” in the nickel lattice at

temperatures above 600 K and by 800 K the helium atom could easily diffuse to the lattice boundary, showing that as temperature increased, the mobility of helium also increased. The diffusion coefficient, and consequently the activation energy, was calculated as a product of the number of helium "hops" and the "hopping" distance, which was the distance between two nearest neighbour octahedral interstitial sites in the nickel structure. The activation energy of the interstitial diffusion of helium in Nickel was found to be 0.48 eV, which was comparable to the experimental value of 0.35 eV. For simulations performed with a palladium lattice, the helium atom began to diffuse at a higher temperature of 800 K due to the closed-shell electronic configuration of palladium. The activation energy was found to be 0.72 eV, leading to a lower diffusion coefficient in palladium than that found for nickel. The group suggests that a higher activation energy is the reason for helium appearing to be less mobile in palladium than in nickel and is also why palladium has a higher helium capacity.

Zu *et al.* simulated the stability of helium in fcc metals; nickel, copper, silver and palladium, by calculating helium formation energies (Zu et al. 2009). *Ab initio* density functional theory (DFT) was used to model the metal lattices, where properties were calculated from first principles. As helium atoms do not interact with the metal lattice, it was suggested that helium atoms should be most stable in a position with the largest free volume, the substitutional position. The position with the smallest free volume is the tetrahedral interstitial position, with the octahedral interstitial position having an intermediate free volume. As expected, it was found that for all fcc metals, substitutional helium

had the lowest formation energy, meaning that helium is most stable when it has replaced a metal atom on a lattice site. For nickel, tetrahedral interstitial helium had a lower formation energy than that for octahedral interstitial helium, which is the reverse of the trend expected. However, when magnetic effects of nickel were excluded, the octahedral interstitial had a lower formation energy than the tetrahedral interstitial. This is as expected because the octahedral interstitial site has a larger free volume than the tetrahedral site, therefore an occupied octahedral interstitial site will cause less disruption to the metal lattice. The formation energies of octahedral and tetrahedral interstitial helium were very similar for copper, suggesting that helium could exist in either site. However, for silver and palladium octahedral interstitial helium again had a lower formation energy than tetrahedral interstitial helium.

Zeng *et al.* studied the migration path of helium within palladium (Zeng et al. 2009). It was found that octahedral interstitials were preferred over tetrahedral interstitials for helium occupation, as octahedral sites had a larger volume and a lower helium formation energy, as also shown by Zu *et al.* (Zu et al. 2009). At low temperatures helium migrated between octahedral sites via an intermediate tetrahedral site, as the migration energy was lower than that of direct migration between two octahedral sites.

As the concentration of helium increases and additional stress is put upon the tritide storage material, the occurrence of crystal defects becomes more frequent. Helium atoms situated close to the material surface cause visual surface roughening (Beavis and Miglioni 1972). As the volume of helium within

the lattice increases, metal atoms are forced to move into interstitial sites and a vacancy, termed a self-interstitial or Frenkel defect, is created in place of the metal atom. The presence of vacancies or additional atoms within interstitial sites can cause rings, known as dislocation loops, where the regular crystal arrangement of the lattice is disturbed.

Gupta compared the density of states of PdT and $PdT_{0.75}He_{0.25}$ to identify the effects of helium evolution on lattice structure (Gupta 2000). For the latter structure, the total lattice was found to expand by 2%. It was also found that as the amount of helium increased, the plateau pressure decreased, meaning that the tritide became more stable. However contrary to other research, Gupta found that the increase in tritide stability was mainly due to the electronic effects of helium and not total lattice expansion. As the tritium within the lattice decayed, tritium from high electronic states was lost, leaving the remaining tritium more tightly bound to the lattice. However, with increasing helium concentration, the lattice became more fragile, as the nearest neighbour palladium atoms no longer sat on their original equilibrium lattice sites, leading to a higher total energy and a large decrease in cohesion energy.

The hypothetical state of PdHe, where all tritium within the metal has completely decayed, was studied by Gupta and Gupta (Gupta and Gupta 2002). As the concentration of helium increased, the metal lattice expanded and the total energy of the system decreased. However, no minimum in the total energy versus lattice parameter plot was found, showing that PdHe

cannot exist and, at a critical helium concentration, the palladium tritide lattice ruptures.

Wang *et al.* simulated the nucleation of helium bubbles in palladium, using an atomistic approach (Wang et al. 2009). They found that helium quickly formed dimers and trimers within the first picosecond of the simulation. By 20 ps, the dimers and trimers combined to form larger clusters. Visualisations and radial distribution functions showed no evidence of palladium within the helium clusters. This was due to vacancies produced by large helium clusters pushing palladium atoms away from their stable lattice sites. The vacancies combined with helium atoms and acted as nucleation sites for the formation of helium bubbles. As more helium atoms combined with the initial cluster, a helium bubble which contained no palladium was formed becoming most stable at 700 K. This mechanism was supported by radial distribution functions which show helium moving towards the centre of mass and palladium moving away from it.

Zeng *et al.* studied the effect of vacancies on helium cluster formation in a palladium lattice (Zeng et al. 2009). Again, it was concluded that a palladium vacancy had a lower helium formation energy than the formation energy of octahedral and tetrahedral interstitial sites. This suggests that helium clusters prefer to form in vacancies, with large vacancies in the metal lattice having the lowest helium formation energy. The helium binding energy increased significantly with increasing helium concentration, with the most stable helium-to-vacancy ratio being 1:1, suggesting that the formation of a new helium

cluster may be preferable to adding to an existing cluster. However, this depends on the presence of vacancies within the palladium lattice, as there were large formation energies when no vacancies were present.

Liu *et al.* simulated the effect of helium clusters on a fcc nickel metal lattice, which is significant as nickel is in the same period as palladium (Liu, Wang et al. 2006). It was found that helium atoms in the vicinity of a lattice vacancy formed a helium cluster with the vacancy acting as a nucleation site. Once the helium cluster included more than 9 helium atoms, the increased volume of the cluster caused nickel atoms to be forced from their original lattice sites, creating self-interstitials. It was also concluded that He_nV_1 clusters with high symmetry, He_6V_1, $He_{16}V_1$ and $He_{24}V_1$, exhibited local maximum binding energies, suggesting that it is difficult to remove helium from stable, high symmetry clusters. Conversely, clusters with an additional helium atom had a local minimum binding energy, as a helium atom can easily be removed to create a more stable, high symmetry cluster. It was also found that at high temperatures, more self-interstitials were created within the metal lattice, caused by greater thermal swelling of the helium cluster than that of the surrounding lattice.

In young metal tritides, there is a low rate of helium loss which can be attributed to helium atoms which exist near to surfaces and grain boundaries and are easily lost from the solid structure (Camp 1977). Beavis and Kass hypothesise two further conditions for helium release;1) the accumulation of helium causing the fragmentation of brittle metals with a high tritium concentration, causing

helium release or 2) helium atoms fill all available tetrahedral and some octahedral interstitial sites, forcing remaining helium to migrate to an interface where helium release occurs (Beavis and Kass 1977). For the latter mechanism, for every 6 – 8 tetrahedral sites available for helium occupation, an additional octahedral interstitial site is also available. Beavis and Kass conclude that the latter interstitial mechanism is the most viable.

Mitchell and Provo experimentally studied helium release from several ErT_x and ZrT_x films at various stages of tritium aging (where x = 1.6 – 1.9) (Mitchell and Provo 1985). Helium content in metal tritides is replenished over time as tritium continues to decay, therefore true helium release rates were found by calculating a release fraction; the ratio of the helium release rate and the helium generation rate. A large average release fraction was found for older tritides in the initial stages of accelerated release, before the release fraction became constant well into the accelerated release stage. It was found that a small number of large helium bursts (10^9 helium atoms) were responsible for the changes in release fraction, especially during the early onset of accelerated release. A single helium bubble composed of 10^9 helium atoms would be 400 nm in size, which is much larger than actual 1 – 2 nm helium bubbles found in metals, as confirmed by transmission electron microscopy (TEM) studies. The helium release bursts were found to have been caused by a correlated, long-range combination of internal fractures, helium bubble bursts and external vibrations and not by the bursting of one large helium bubble. At low helium concentrations, before accelerated release, small amounts of isolated helium atoms were released via a theoretical diffusion

model, where individual helium atoms migrate to the metal surface and are released. However, this model does not hold for the larger helium bursts seen during accelerated release. For both the diffusion model and the accelerated release case, the rate of helium release was found to be temperature dependent, as many helium atoms are deeply trapped within bubbles and are only released at high temperatures. Also for both cases, the release fraction was found to abruptly increase immediately after external striking of the metal, especially prior to accelerated release, causing internal vibrations and therefore a temporary increase in helium release.

1.4 Material Applications

Tritium can be used in nuclear fusion in which deuterium and tritium atoms react to form a heavier helium atom, a neutron and produce an extremely large release of energy, on the scale of 17 MeV. Tritium is also an important component of hydrogen bombs, where fusion reactions provide a source of neutrons, leading to a chain of fission reactions.

Palladium hydride plays an important role in the search for future "green" energy technologies and reduction of greenhouse gas production, as it is a promising hydrogen storage material. However, the percentage weight of hydrogen in $PdH_{0.6}$ is 0.56 (Schlapbach and Zuttel 2001), which is lower than values found in other metal hydrides, particularly MgH_2 which has a hydrogen percentage weight of 7.60 (Adams and Chen 2011). Despite a relatively low density of hydrogen, palladium hydride shows promise as a component in metal-alloy hydrides, as it can absorb and desorb hydrogen gas at room

temperature (Joubert and Thiebaut 2009), compared to MgH_2 which has an absorption temperature almost double that of $PdH_{0.6}$ (Adams and Chen 2011). Along with an absorption temperature of 298 K, a low pressure of 0.02 bar is required for hydrogen sorption in palladium metal (Schlapbach and Zuttel 2001). In other hydrides, which have a large capacity for hydrogen, hydrogen sorption occurs at both high pressures and high temperatures, such as 313 K and 10 bar for the case of TiV_2H_4, significantly increasing operating costs. In order to improve hydrogen sorption in metal hydrides, a thin outer layer of palladium can be added to the material, exploiting both ambient sorption conditions and high storage capacities (Adams and Chen 2011). Pure bulk palladium hydride is also inconvenient due to the extremely high cost and relatively low abundance of palladium metal, however this may be overcome by the synthesis of palladium nano-particles or Pd-M alloys.

Industrially, palladium is a key component in hydrogen and deuterium gas purification (Holder and Wermer 1995). Extremely pure hydrogen gas is essential in hydrogen fuel cells for the combustion of hydrogen gas in the presence of oxygen gas, leading to the production of water vapour with no unwanted by-products or pollutants. Palladium metal facilitates gas purification via the energy efficient absorption and desorption of hydrogen gas on the palladium surface.

Hydrogen gas detection takes advantage of the distinctive transition from α-phase PdH to β-phase PdH, by measuring lattice expansion as well as an increase in electrical resistivity (Adams and Chen 2011). Also, well known

pressure-composition isotherms are useful in determining the pressure of the detected hydrogen gas.

Tritium is a waste product from nuclear fission reactions and palladium offers safe, long-term tritium storage, with lifetimes of up to 19 years before mechanical failure (Zeng et al. 2009). Palladium plays a key role in tritium purification, with pure tritium being a component for possible nuclear fusion reactions.

1.5 Modelling Tritides

Clearly, practical experiments involving tritium are dangerous and lengthy due to a long half-life, meaning that accurate computer simulations are essential for the progression of tritium research. In the past 20 years, as computational techniques and processor power have improved, focus has shifted from experimental research to computational methods, which now account for the majority of tritium-based research. Computational techniques also provide a good method for studying microscopic processes during tritium decay, such as the diffusion of helium atoms within a metal lattice, which may otherwise be unobservable directly experimentally.

Wang *et al.* used Molecular Dynamics with an NVT ensemble, where number of particles (N), volume (V) and temperature (T) of the system were kept constant, to simulate helium bubble formation in palladium metal (Wang et al. 2009). 55 helium atoms were placed in different octahedral interstitial sites within the metal lattice, analogous to the experimental ion implantation method

where no tritium is present. Modified analytical embedded atom method (MAEAM) (Yang et al. 2004), Morse (Baskes and Melius 1979) and Lennard-Jones (Johnson 1973) potentials were used to describe the interactions of Pd-Pd, Pd-He and He-He respectively. Period boundary conditions were employed in all directions except the (0 0 1) direction, where free boundary conditions were subjected, representing the palladium metal surface. Radial distribution functions and visulisations of helium and palladium were combined to follow the time evolution of the helium clusters. It was found that at 300K, helium began to aggregate into clusters, with larger helium clusters, or bubbles, formed at higher helium concentrations. It was suggested that helium bubble formation and growth could be accelerated by increasing the temperature of the system.

Liu *et al.* used MD with constant temperature to simulate helium clustering in a nickel metal lattice (Liu et al. 2006). Again, different potentials were used to describe different atom interactions, in this case, Ackland (Ackland et al. 1987), Melius (Melius et al. 1978) and Beck (Beck 1968) potentials were used for Ni-Ni, Ni-He and He-He interactions respectively. The potentials were verified by calculating the formation energies of a vacancy and an interstitial helium atom, with the values obtained being in good agreement with experimental values.

Gupta (Gupta 2000, Gupta and Gupta 2002) studied the effects of helium atoms within palladium tritide, using *ab initio* electronic structure calculations with the linear muffin-tin orbitals method (LMTO) (Andersen 1975). A simple cubic cell with 4PdT was modelled, with Pd atoms occupying the corners and

face centres of the cell. Tritium atoms occupied the octahedral interstitial sites of the lattice, located in the middle of each cell edge and the centre of the cell. A system in which one tritium atom had randomly decayed to helium was studied ($PdT_{0.75}He_{0.25}$) where, for simplicity, the central tritium atom was replaced with a helium atom. Local density approximations (LDAs) used in this work were found to overestimate the lattice parameter by 3% compared with experimental values. Typically, LDA underestimates lattice parameters, due to an overestimation of binding energies.

Xia *et al.* performed 1 ns MD simulations to compare the diffusion of a helium atom in palladium and nickel lattices at increasing temperatures (Xia et al. 2006). A box of 864 metal atoms and one helium atom was constructed and periodic boundary conditions were employed. An NVE ensemble (constant number of particles (N), volume (V) and energy (E)) was used with an embedded-atom method (EAM) (Daw and Baskes 1983) to describe interactions between atoms, where helium-metal interactions were fitted to experiment. The helium atom was allowed to randomly "hop" between octahedral interstitial sites in the metal lattice. The jump-frequency method was used to calculate the diffusion coefficient and activation energy of helium diffusion in each metal.

Yang *et al.* calculated the formation energy and binding energy of helium-vacancy clusters in nickel and palladium lattices (Yang et al. 2004). EAM (Daw and Baskes 1983) was used to describe metal-metal interactions, a Lennard-Jones potential (Emig et al. 1992) was used for helium-helium interactions and

helium-metal interactions were described by free-electron helium-metal pair potentials. All atoms were relaxed using an annealed molecular dynamics method. Vacancies were produced by creating a single vacancy initially, then repeatedly removing metal atoms with the largest potential energy. The helium binding energy was calculated by using Equation 1-2.

Equation 1-2: The binding energy of a helium atom within a host lattice. (Yang et al. 2004)

$$E_B(He) = E_f(He_{n-1}V_m) + E_f(He) - E_f(He_nV_m)$$

The calculated binding energy of helium was considered viable, as it was comparable to values obtained by Wilson *et al. (Wilson 1983).*

Ruda *et al.* used Monte Carlo (MC) simulations, with constant temperature, pressure, hydrogen chemical potential and number of metal atoms, to compare hydrogen absorption in nanoparticle and bulk palladium systems (Ruda et al. 2010). Modified EAM (Zhou et al. 2008) was used to represent atomic interactions and a hydrogen reservoir with constant temperature and pressure was included to allow for the open absorption and desorption of hydrogen. Just under half of the total simulation steps were used for relaxation of the system, with the remaining steps used to simulate the creation and destruction of hydrogen atoms. For the bulk system, a hydrogen atom was positioned in each octahedral interstitial site of the metal lattice. For the nanoparticle systems, spherical crystallites with radius 1 nm and 2 nm were created and the hydrogen atoms randomly positioned within the crystals. For the nanoparticle systems it

was found that hydrogen was absorbed mainly into the subsurface region of the metal crystals.

The extensive use of EAM or modified EAM in almost all metal tritide/hydride systems is of significant value and suggests that the EAM potential is highly effective for modelling metal-metal and metal-hydrogen interactions with little or no modification needed. Daw and Baskes developed EAM, where each atom was considered as an impurity, embedded in a host lattice consisting of all other atoms in the system (Daw and Baskes 1983). The embedding energy was determined by calculating the electron density of the host lattice both with and without the impurity atom present, which allowed for the inclusion of energy contributions from intrinsic defects and cracks. For simplicity, a local approximation was applied where only the local environment of the impurity atom has an effect on the embedding energy. The total energy of the system was calculated by two functions, which were fitted to experimental data, as shown in Equation 1-3.

Equation 1-3: The Embedded Atom Method (EAM) - A local approximation of the total energy of a system with defects in a host lattice, where the first term is the electron density at the impurity site and the second term is a short-range electrostatic pair potential. (Daw and Baskes 1983).

$$E_{tot} = \sum_i F_i(\rho_i(R_i)) + \frac{1}{2}\sum_{i,j}\varphi(R_{ij})$$

The first term in Equation 1-3 represents the electron density at the impurity site, where ρ_i is the electron density of the host lattice without impurity atom, i.

The second term is an electrostatic interaction, where φ is a short-range electrostatic pair potential. EAM was tested by determining the amount of stress required to cause critical failure to a semi-infinite slab of nickel atoms which contained a crack, produced by intentionally removing four nickel atoms from the centre of the slab. As hydrogen atoms were added to the system, the critical stress energy decreased from 0.13 to 0.09 eV/Å^3, particularly when hydrogen atoms were located close to the crack. This suggests that the presence of hydrogen in a metal lattice, especially if the hydrogen atoms are located on or near intrinsic defects, leads to a weakening of the lattice.

The embedded atom method (EAM), or modified EAM, has been used extensively in computational studies of palladium hydride, due to the effective description of metal-metal and metal-hydrogen interactions (Zimmerman et al. 2007, Zhou et al. 2008). In EAM, an atom is treated as an impurity which is embedded in a host lattice, formed from the remaining atoms in the system. The electron density of the system with and without the embedded atom is calculated, leading to the quantitative measurement of energy contributions from the embedded atom.

Pratt and Eckert performed a molecular dynamics (MD) simulation on $PdH_{0.004}$ using the EAM. The precision of the simulation allowed for accurate calculation of the relaxed atomic coordinates of hydrogen, which are found to deviate slightly from the center of the octahedral interstitial site (Pratt and Eckert 1989).

In contrast, Gillan used simple interaction potentials in an MD simulation of palladium hydride. From this the diffusion pathway of hydrogen was

determined by calculating the energy of the system at each hydrogen position (Gillan 1986).

Some studies of palladium hydride have combined both experimental research and computational calculations in order to obtain a wider range of properties. Hemmes et al. used experimental pressure experiments, as well as calculating electronic band structures computationally, to draw conclusions on the pressure dependence of the critical temperature of palladium hydride (Hemmes et al. 1989).

1.6 Aims of this Work

Clearly, any future research conducted on palladium tritide systems must complement and build upon previous works.

Computationally, small metal tritide systems tend to be modelled using Density Functional Theory, Larger computational simulations, such as those concerning helium migration and tritium absorption, use Molecular Dynamics methods to describe the evolution of atoms, particularly using the Embedded Atom Method (EAM) to model metal-metal and metal-hydrogen/tritium interactions.

The main aim of this research is to carry out a thorough investigation into the structure of palladium hydride, using rigorous computational methods. Ultimately, an accurate model with the experimental molecular formula $PdH_{0.7}$ is to be produced, therefore enabling the calculation of energetic and thermodynamical data which is comparable with experimental findings.

Palladium hydride and palladium tritide have been studied experiementally, particularly in the 1970s and 1980s and mostly concerning the lifetime of the material, known as tritium aging. More recently there have been some computational studies on palladium hydride focusing on hydrogen absorption, and pressure composition isotherms. There have been few computational studies on palladium tritide, with studies instead focusing on pure palladium metal with helium atoms. This work aims to complement the existing work in the literature by modelling palladium tritide with helium atoms, rather than palladium metal.

Palladium is an ideal candidate for use as a metal tritide, as the potential for long-term tritium storage has already been identified. Simulations to determine a critical tritium concentration in palladium are useful in determining the point at which mechanical failure occurs. However, it is necessary to perform subsequent calculations with a tritium concentration well below the critical concentration, as the effects of an increase in helium concentration over time must also be taken into consideration.

Hydrogen absorption in a metal is an excellent starting point for the simulation of metal tritides, as tritium is an isotope of hydrogen, suggesting that the absorption mechanisms would be very similar. Hydrogen atoms are computationally cheap and are easily modelled. However, due to the high weight to atomic radius ratio of hydrogen, isotope effects must also be taken into consideration, as tritium is heavier than hydrogen and possesses stronger covalent bonds. Many studies have been conducted on the hydrogen

absorption of palladium powders, but little research has been undertaken concerning bulk palladium or palladium thin films. For hydrogen absorption in bulk palladium, the surface structure of the metal lattice must also be taken into consideration, as different surfaces have different structures and different shaped absorption sites.

The presence and effects of helium on the metal lattice are an integral part of the study of metal tritides. The migration and bubble formation of helium are extremely important consequences of tritium decay and have been researched extensively. The calculation of formation and binding energies plays a large part in comparing the stability of different helium positions, leading to conclusions on mechanisms of helium migration. However, few studies have been conducted on the behaviour of helium in a metal tritide lattice; instead helium is studied in metal lattices with no tritium present. It is important to consider which interstitial sites helium will occupy if tritium atoms are occupying a proportion of the interstitials.

Very little research has been conducted on desorption of tritium from a metal lattice. It is important to consider any mechanical or microscopic structural damage caused by the safe removal of tritium from a storage material.

Therefore, future research should initially concern hydrogen absorption into a palladium lattice, before using DFT methods to model small palladium tritide systems. MD simulations should then be undertaken to study the time evolution of both helium migration and helium bubble formation. Finally, tritium

desorption should also be studied to investigate the occurrence of any significant metal lattice damage.

There is an absence within the literature concerning the study of the stability of hydrogen or tritium vacancies within palladium hydride/ tritide. Therefore an in-depth analysis is to be undertaken using DFT to investigate the occurrence and potential clustering of hydrogen vacancies within different configurations of palladium hydride. It is hoped that any observed trends can be utilized throughout this work with different computational methods and a range of cell sizes.

Although Jigato et al. have modelled the {111} surface of palladium hydride, no work has been undertaken to study all common surfaces of palladium hydride. This work aims to explore all of the common surfaces of palladium hydride (both stoichiometric PdH and non-stoichiometric PdH_x), namely {100}, {101} and {111} surfaces. This work will present novel findings on these surfaces.

Finally, this work proposes to be the first to model the interaction of a palladium hydride grain boundary with water molecules, as currently this interaction is not discussed in the literature.

Chapter 2 discusses the theory behind the methodologies used in this work, namely Density Functional Theory, interatomic potential derivation and Molecular Dynamics.

Chapters 3 – 6 explore the results obtained in this work relating to electronic properties, interatomic potentials, surfaces and grain boundaries of stoichiometric and non-stoichiometric palladium hydride/tritide. *Ab-initio* DFT calculations of unit cells, interatomic potential derivation and surface structures were relatively small, simple systems which were studied using a standard desktop computer. Calculations involving larger systems such as 2x2x1 or 2x2x2 supercells (containing 32 and 64 atoms respectively) and molecular dynamics studies (containing hundreds of atoms) were performed on UCL computer clusters (Legion and Huygens).

Finally, Chapter 7 acts as a discussion in order to further explain key findings as well as suggest further work.

Chapter 2

Theory of Computational Modeling

The electronic properties of palladium hydride were explored using Density Functional Theory (DFT). This modelling technique was also used to study palladium tritide and helium-3, the decay product of tritium. From the DFT data obtained, an interatomic potential was developed to describe the palladium – hydrogen interaction and explore the surfaces of palladium hydride. Finally, Molecular Dynamics (MD) was used to study palladium hydride grain boundaries.

2.1 Density Functional Theory

The Schrödinger equation describes the kinetic and potential energy for both nuclei and electrons in an atomic or molecular system. The equation can be solved exactly for one electron systems. However, this equation can only be approximated for molecular systems with many electrons. The equation can be further expanded with respect to particle position and momentum.

Equation 2-1: Time-independent Schrodinger equation, where H is the Hamiltonian operator, Ψ is the wavefunction, E is the energy and τ are particle positions and momenta.

$$H\Psi = E\Psi$$

$$H(\tau_1,\tau_2...\tau_N)\Psi(\tau_1,\tau_2...\tau_N) = E\Psi(\tau_1,\tau_2...\tau_N)$$

Where H is the Hamiltonian operator, Ψ is the wavefunction, E is the energy and τ are particle positions and momenta.

The Hamiltonian can be described as the sum of the kinetic and potential energy, which can be further broken down into components which describes the interactions between the nucleus and the electrons.

Equation 2-2: The Hamiltonian with respect to nuclear and electronic energy, where T_e represents the kinetic energy of the electrons, T_n is the kinetic energy of the nuclei, V_{ne} is nuclear-electron attraction, V_{ee} is electron-electron repulsion and V_{nn} represents nuclear-nuclear repulsion.

$$H = T_e + T_n + V_{ne} + V_{ee} + V_{nn}$$

T_e represents the kinetic energy of the electrons, T_n is the kinetic energy of the nuclei, V_{ne} is nuclear-electron attraction, V_{ee} is electron-electron repulsion and V_{nn} represents the nuclear-nuclear repulsion.

For simplicity, the electrons and nuclei are treated separately, leading to the Born-Oppenheimer approximation which states that nuclei have a much larger

mass than electrons, therefore the motion of the nucleus is very slow. The kinetic energy of the nuclei can be estimated to equal zero. The Schrödinger equation can now be solved for a set of electrons in a field of fixed nuclei.

Equation 2-3: The Hamiltonian with respect to electrons only, where T is the kinetic energy of an electron, U is the interaction between electrons and V is the interaction between an electron and the field of fixed nuclei.

$$H = T + U + V$$

Where T is the kinetic energy of an electron, U is the interaction between electrons and V is the interaction between an electron and the field of fixed nuclei.

Density functional theory attempts to solve the electronic part of the Schrödinger equation by calculating the electron density and the total electronic energy. A simplified description of the total electronic energy is shown in Equation 2-4.

Equation 2-4: Total electronic energy as a function of electron density (p(r)) and electronic energy (V).

$$E[p(r)] = \int V_{ext}(r)\,p(r)dr + F[p(r)]$$

Where p(r) is the electron density of electrons with coordinates r. The function, F[p(r)] can be further broken down into;

$$F[p(r)] = E_{KE}[p(r)] + E_{H}[p(r)] + E_{XC}[p(r)]$$

Where E_{KE} is the kinetic energy of a set of imaginary, non-interacting electrons, which possess the same electron density as the actual system. E_H is the electron-electron Coulombic repulsion energy and E_{XC} represents the exchange-correlation function. The exchange correlation function describes electron – electron interactions in the system.

The electron density of the system is calculated by measuring the density of imaginary one-electron orbitals called Kohn-Sham orbitals (Kohn and Sham 1965). The total energy of the system can be obtained by determining the electron density, p(r), which is a function of an electron with coordinates r.

Equation 2-5: Electron density as described by Kohn-Sham orbitals, where p(r) is the electron density, χ is a (basis) set of orbitals and C is an unknown coefficient. (Kohn and Sham 1965)

$$p(r) = \chi_{\mu} C_{\mu i}$$

Where p(r) is the electron density, χ is a (basis) set of orbitals and C is an unknown coefficient.

The total electronic density can then be determined by the summation all Kohn-Sham orbitals, as shown in Equation 2-6.

.

Equation 2-6: The summation of Kohn-Sham orbitals, leading to an approximation of total electronic density by a self consistent approach. (Kohn and Sham 1965)

$$p(r) = \sum |\chi_\mu|^2$$

From Equation 2-6 it can been seen that the electron density, and therefore the energy, of the orbitals depends on the choice of orbitals themselves, therefore requiring the need of a self-consistent approach. An initial estimation of the electron density of the system is made, leading to a set of Kohn-Sham orbitals. From this, a hopefully improved electron density is then calculated. Again, a set of orbitals are derived from the new electron density. The process is repeated until energy convergence is reached.

The accuracy of a calculation depends significantly on the estimation of the electron exchange-correlation energy. Electron exchange occurs when one electron swaps position with another electron. Electron correlation describes the interaction between one electron and all other electrons in the system. The exchange and correlation energy can be accurately determined for a uniform electron gas. There are two approaches to estimating this energy value; using non-empirical functionals or using semi-empirical functionals. An example of the former method is the Local Density Approximation (LDA), where the electron density is estimated to be constant across the whole system and the functional is fitted to the energy of the uniform electron gas. The latter method can be performed using the Generalised Gradient Approximation (GGA), which calculates both the electron density and its gradient at each point in space,

with the exchange-correlation energy being fitted to experiment. GGA acts as an improvement to LDA when describing a system containing d- or f-orbitals. The exchange correlation energy for highly localised f-oribital elements should be further corrected using the DFT+U method. However, as no f-orbitals are present in palladium hydride, GGA exchange-correlation energy is sufficient for this work.

DFT calculations are generally performed at 0 K in a vacuum, with the system existing in the minimum energy state only, known as the ground state. DFT gives a good approximation of the total energy of a system, however it cannot calculate experimental total energies exactly. This shortfall can be explained by the electron self-interaction problem, where an electron artificially interacts with itself.

The Brillouin zone is a version of the unit cell in reciprocal space, where k is the wave vector. In order to calculate the wavefunction exactly, we must solve the wavefunction for every possible value of k. This problem can be further simplified by sampling the Brillouin zone with a finite number of k-points within in a Monkhorst-Pack grid (Monkhorst and Pack 1976). A large number of k-points produces a finer grid and therefore a more accurate calculation, however too many k-points leads to a computationally expensive calculation.

In order to solve the Kohn-Sham equations and therefore describe the wavefunction, two types of basis set can be used; localised basis sets, such as Slater Type Orbitals (Slater 1930) and Gaussian Type Orbitals (GTO) (Boys 1950), or the plane wave basis set. In the localised basis sets, one electron

orbitals relate to the atomic orbitals of each atom. The plane wave basis set is the sum of a number of plane waves, meaning that the system is no longer represented by atomic orbitals. This requires an infinite number of plane waves to be calculated, however this can be approximated by using a plane wave cut-off, where the plane waves with the highest kinetic energies, those representing the core electrons, are excluded. The use of pseudopotentials enables the implementation of a plane wave cut-off.

Each atom can be described by a pseudopotential, where the nucleus and core electrons of each atom are approximated by an effective potential, meaning that only the valence electrons are required to be described by wavefunctions. The pseudopotential is required to describe the interaction between the “core” (i.e. the nucleus and the core electrons) and the valence electrons.

In order to determine the local energy minimum of the system, a conjugate gradient algorithm can be used. This is where many “steps” down the gradient of the potential energy surface are taken until the local energy minimum is reached.

2.2 Interatomic Potential Derivation

As well as the use of pseudopotentials, the interaction between two atoms can be described by interatomic potentials, of which there are many varieties studied in the literature. The Buckingham potential (Buckingham 1938) has been used extensively to model ionic materials and so was chosen for use in this work.

The first two terms of the Buckingham potential represent the repulsion interaction between the two ions, whereas the final term represents Coulombic attraction.

Equation 2-7: The Buckingham potential describing the Coulombic repulsion (A and ρ) and Van der Waals attraction (C) between two atoms, where r is the ionic radius of each atomic species.

$$\Psi_{12}(r) = Aexp(-\rho r) - \frac{C}{r^6}$$

Where A and ρ represent Coulombic repulsion, C represents Van der Waals attraction and r is the ionic radius of each species. These terms are specific to each interatomic interaction and are fitted to experimental data.

In order to represent the atoms within an interatomic potential, two different methods are mainly used; rigid ion theory and the core-shell model. Within the rigid ion theory, both the nucleus and electrons of an atom are approximated by a single point charge. In the core-shell model, an atom is represented by both a core and a shell, where the core represents the nucleus and core electrons and the shell represents the valence electrons. The shell is attached to the core by a harmonic spring and the charge of the atom is shared between the core and polarisable shell. The atomic coordinates of the core and shell are estimated to be the same, meaning that the shell sits directly on top of the core.

In order to fit to experimental or *ab-initio* data the method of least squares fitting is undertaken. Many iterations of a least squares fitting method are undertaken

to minimise the sum of the square of the residuals, where residuals are the difference between the experimental or *ab-initio* values and the fitted value derived by the potential.

Elastic Constants describe the stress and strain of a material, as shown in Equation 2-8.

Equation 2-8: Elastic constant of a material as a function of stress and strain.

$$\sigma_{ij} = \sum c_{ijkl}\varepsilon_{kl}$$

As palladium hydride is cubic, symmetry considerations mean that only C_{11}, C_{12} and C_{44} elastic constants are required to be calculated.

2.3 Molecular Dynamics

One drawback to Density Functional Theory is that calculations of larger systems with hundreds or thousands of atoms is computationally expensive, whereas Molecular Dynamics (MD) can model a large system cheaply. However, the resulting data can be very different and the correct technique should be used for the correct purpose; DFT is the preferred method for calculation of electronic properties, whereas interatomic potentials and Molecular Dynamics (MD) are more frequently used to investigate structural and mechanical properties, as well as atomic interactions over hundreds of nanoseconds. When undertaking an extensive review of a material, as posed in this work, it is preferable to use a variety of computational techniques in order to report a wide range of properties.

Classical Molecular Dynamics (MD) is achieved by solving Newton's equations of motion in order to study how molecules within a system move over time. This is where the force acting on an atom is related to the position and momentum of the atom.

Equation 2-9: Newton's second law of motion where x is the position of the atom, m is the mass of the atom and F is the force acting on the atom.

$$F = m\frac{d^2x}{dt^2}$$

Where x is the position of the atom, m is the mass of the atom and F is the force acting on the atom.

When studying a many particle system, each particle will influence the force acting on another particle. Therefore Newton's equations must be expanded:

$$F(x_1, x_2 \ldots x_N) = m\frac{d^2x}{dt^2}$$

The position and velocity of an atom is required to be calculated iteratively during the simulation, in order to accurately describe the system over time. To integrate the equations of motion for a complex system where atoms interact with many other atoms, an algorithm is required, namely the Verlet algorithm (Verlet 1967). The position and velocity of each atom is recalculated at distinct points in time based on the timestep (Δt) of the simulation.

The Verlet equations below describe the position and velocity of an atom at time, t.

Equation 2-10: The Verlet algorithm relating to the position (x) and velocity (v) of an atom at a distinct time (t) in the simulation.

$$x(t+\Delta t) = x(t) + v(t)\Delta t + \frac{1}{2}a(t)\Delta t^2 + \frac{1}{6}b(t)\Delta t^3 + O(\Delta t^4)$$

$$x(t-\Delta t) = x(t) - v(t)\Delta t + \frac{1}{2}a(t)\Delta t^2 - \frac{1}{6}b(t)\Delta t^3 + O(\Delta t^4)$$

These equations can be combined:

$$x(t+\Delta t) = 2x(t) - x(t-\Delta t) + a(t)\Delta t^2 + O(\Delta t^4)$$

The previous position and velocity of the atom at (t – Δt) is used to determine the force acting on an atom, which leads to the calculation of the velocity of the atom at the current time (t) and the future position of the atom at (t + Δt). This means that the known velocity of an atom is always one timestep behind the known position of the same atom.

The simulation package used in this work DLPOLY 2.20 (Smith, 2006, Todorov, 2006) employs a modified version of the Verlet algorithm, called the Verlet Leapfrog algorithm. Here, the position is calculated at every timestep (t + Δt), whereas the velocity is calculated at every half-timestep (t + ½Δt).

For each simulation, an appropriate timestep must be chosen; if the timestep is too large, the atoms will move a large distance between each timestep and if the timestep is too small, the calculation will be computationally expensive.

The thermodynamics of the system are calculated using an ensemble. The ensemble describes many configurations of a system (i.e. the same system with different atom positions and velocities) which have the same macroscopic properties. It is assumed that many different configurations at the same point in time are equivalent to one configuration over a length of time. The ensemble takes an average of the thermodynamic properties of the configuration over the length of the simulation.

A variety of ensembles are possible, of which the most widely used are the micro-canonical ensemble (NVE), the Canonical ensemble (NVT) and the isothermal-isobaric ensemble (NPT). The three letter acronym of the ensemble indicates which properties are to remain constant in the simulation, therefore the NVE ensemble has a constant number of atoms; constant volume of the simulation box and constant total energy of the system, whereas the NPT ensemble has a constant number of atoms, constant pressure and constant temperature. Other properties which are not included within the ensemble are free to change with simulation time. The constant temperature ensembles used in this work employ the Nosé-Hoover thermostat (Hoover 1985).

Each molecular dynamics simulation should be equilibrated for an extended simulation time before the measurement of any properties of the system.

Simulating a bulk system with billions of atoms would be impossible computationally, therefore a method of replicating the bulk with only hundreds or thousands of atoms must be used. Periodic Boundary Conditions (PBC) allow for the simulation of large bulk-like systems by repeating images of the simulation box (and the atoms contained therein) in all three directions in space. The interaction of an atom and the nearest image of its neighbour can then be studied, meaning that the two atoms are not necessarily in the same image box. However, the simulation box must be large enough to ensure that the atom does not interact with an image of itself.

Chapter 3

Density Functional Theory Modelling of Palladium Hydride, Tritide and Helium-3

3.1 Introduction

Using crystallographic data (Maeland and Flanagan 1964), palladium and hydrogen atom coordinates and lattice constants were determined for use in subsequent calculations. Lattice constants of 4.040 Å were used for all palladium hydride systems and 3.890 Å for a pure palladium system.

DFT calculations were performed using the Vienna Ab-initio Simulation Package (VASP 5.2.12) (Kresse and Hafner 1993, Kresse and Hafner 1994, Kresse and Furthmuller 1996, Kresse and Furthmuller 1996). Perdue Burke Ernzerhof (PBE) pseudo-potentials (Perdew et al. 1992, Perdew et al. 1993), a type of generalised gradient approximation (GGA), were used to describe the electronic structure of palladium, hydrogen and helium atoms.

Standard hydrogen and helium Perdew, Burke and Emzerfhof (PBE) pseudo-potentials were used in the *ab-initio* calculations, where the mass was manually modified to have an atomic mass of 3 instead of 1 and 4 respectively. Two varieties of palladium PBE pseudo-potentials were found. The first variety

treated the 4p and 4d electrons as valance electrons, whereas only 4d electrons were treated as valence electrons the second variety of potential. DFT calculations of a unit cell of PdH were performed in order to compare each palladium potential. The pseudopotential with less valence electrons was found to be less computationally expensive, whilst producing very similar results to the pseudopotential with more valance electrons. therefore from this point the pseudo-potential with 4d valence electrons only was used to represent the electronic structure of palladium.

Geometry optimisations, leading to a minimised total energy, were carried out for each system using a conjugate gradient algorithm, where many “steps” down the gradient of a potential energy surface are taken until the local energy minimum is reached. During geometry optimisation, all atoms and lattice parameters were allowed to relax fully.

In order to determine if the effect of Van der Waals forces are significant in palladium and palladium hydride systems, lattice parameters including and excluding Van der Waals forces were calculated. Table 3-1 compares experimental lattice parameters of palladium and palladium hydride, with calculated values using different versions of VASP and both with and without considering Van der Waals contributions.

Table 3-1: Comparison of experimental lattice parameters of palladium and palladium hydride systems with lattice parameters calculated by DFT whilst including and excluding Van der Waals contributions.

Vasp version	Pd lattice parameter (Å)	PdH lattice parameter (Å)
4.6 (no VdW)	3.9546	4.1405
5.2.12 (no VdW)	3.8889	4.0817
5.2.12 (VdW) (VdW-DF functional)	3.94	4.1405
Experimental (Maeland and Flanagan 1966)	3.89	4.040[a]

[a] - The experimental equilibrium formula of palladium hydride is approximately $PdH_{0.7}$, whereas DFT calculations were applied to stoichiometric PdH

The lattice constant for Pd metal calculated using VASP 5.2.12 with no Van der Waals contributions was 0.0011 Å lower than the corresponding experimental value. Overestimation of the calculated palladium hydride lattice parameter was due to the difference between computational and experimental formulas, which were PdH and $PdH_{0.7}$ respectively, as a higher hydrogen content leads to a larger unit cell volume. Lattice parameters calculated using VASP 5.2.12, particularly when Van der Waals contributions were not included, were found to be closer to experimental values than those calculated using VASP 4.6.

Although the inclusion of Van der Waals forces may be advantageous for some systems, in palladium metal and palladium hydride systems the exclusion of Van der Waals forces leads to lattice parameters closer to experimental results. Also, calculations including Van der Waals force contributions were required to be optimised manually, due to the lack of an effective optimisation algorithm. This may lead to less accurate lattice parameters and a large number of expensive calculations. For these reasons, Van der Waals contributions have not been included in this work. Unless otherwise stated VASP 5.2.12 was used in this work for all DFT calculations.

The number of k-points required for the system was determined by performing individual DFT calculations on a PdH system with an increasing number of k-points. An appropriate number of k-points were reached when total energy convergence to 1 meV per atom was observed (as shown in . For all 2x2x1 palladium hydride and palladium metal supercells, a k-point mesh of 4x4x8 was used, with a 8x8x8 k-point mesh being used for unit cell calculations.

An appropriately high plane wave cut-off energy of 660 eV was chosen by total energy convergence, so that the small number of plane waves with an energy above this value were excluded. The maximum number of ionic steps for each calculation was set to 200. Total energy convergence was achieved for each calculation when a total energy difference of 3.0E-4 eV between two steps was reached, as shown in Table 3-2.

Table 3-2 - Energy cut-off convergence for a unit cell of palladium hydride (PdH) leading to an energy cut off of 660 eV.

Energy Cut-off (eV)	Total Energy (eV)	ΔE
400	-31.3235	
600	-31.3503	0.0268
650	-31.3525	0.0022
660	-31.3528	0.0003
670	-31.3531	0.0003

In order to calculate palladium hydride formation energies ($\Delta_f H$) in Section 3.2, the following equation was used:

$$\Delta_f H_{(PdHx)} = E_{tot(PdHx)} - E_{tot(Pd)} - x\frac{E_{tot(H_2)}}{2}$$

The total energy of H_2 was calculated in VASP by modelling two hydrogen atoms at a distance of 0.74 Å (which equates to the hydrogen-hydrogen bond length) in a 10x10x10 Å box, with a 1x1x1 k-mesh. The total energy of H_2 was found to be -6.6597 eV.

It was not possible to calculate formation energies of cells containing helium,

as an isolated helium atom had not been modelled.

3.2 Configurational Analysis

Hydrogen vacancies were artificially created in a palladium hydride system by manually removing between one and five hydrogen atoms. To achieve a molecular formula close to that found for experimental palladium hydride ($PdH_{0.7}$), a large number of hydrogen vacancies are required within a relatively small computational cell. For example five hydrogen vacancies must exist within a 2x2x1 32-atom supercell, namely 16 palladium atoms, 11 hydrogen atoms and 5 hydrogen vacancies. As shown in Table 3-3 there are a significantly large total number of configurations for 2x2x1 supercells containing four or five hydrogen vacancies, as there are a vast number of combinations in which the vacancies can be arranged within the supercell. Clearly, it is both impracticable and computationally expensive to perform calculations on each of these configurations, requiring the use of an effective method to greatly reduce the number of configurations.

An in-house program, Site-Occupancy Disorder (SOD 0.26) (Grau-Crespo et al. 2007), was used to reduce the total number of configurations for each system. The SOD code uses the space group of the parent structure and the required number of vacancies to determine all possible symmetry operations including rotations, reflections and transformations. This leads to a list of all possible configurations. A list of unique configurations is then constructed by exploring all possible symmetry operations and excluding configurations which are symmetrically equivalent. Essentially, identical configurations are

eliminated, reducing the number of configurations significantly, as shown in Table 3-3. Density Functional Theory energy minimisation calculations were then performed on each unique configuration. The formula range shown in Table 3-3 is equivalent to the β-phase of palladium hydride as shown in Figure 1-4. Additionally, the formula $PdH_{0.6875}$ is found to be close to that of the experimentally stable formula of $PdH_{0.7}$ (Maeland and Flanagan 1966).

Table 3-3: The introduction of hydrogen vacancies into a 2x2x1 palladium hydride supercell, leading to an increase in the total number of possible

configurations. Demonstration of the number of unique configurations as determined by the Site-Occupancy Disorder code.

Number of Hydrogen Vacancies	Molecular Formula	Total Number of Configurations	Number of Unique Configurations	Average Total Energy (eV)	Average Energy of Formation ($\Delta_f H$) (eV)
0	PdH	1	1	-138.8900	-52.9954
1	$PdH_{0.9375}$	16	1	-135.0100	-49.3235
2	$PdH_{0.875}$	120	5	-131.7678	-46.2894
3	$PdH_{0.8125}$	560	10	-128.4637	-43.1934
4	$PdH_{0.75}$	1820	33	-125.1196	-40.0574
5	$PdH_{0.6875}$	4368	53	-121.7392	- 36.8851

Table 3-3 shows that the average total energy increases as the number of hydrogen vacancies increases, suggesting that the stoichiometric PdH system is the most energetically favourable. As $PdH_{0.6875}$ is similar to $PdH_{0.7}$, the configurations of this formula were selected for further analysis. It is not clear from the literature as to why $PdH_{0.7}$ is the stable molecular formula for β-phase palladium hydride. By exploring the different configurations of the non-

stoichiometric material, it may be possible to further understand this phenomenon. Figure 3-1 shows the total energy of the 53 unique configurations of $PdH_{0.6875}$. The difference in energy between the highest and lowest energy configurations was found to be 0.14 eV. The configurations with notably high and low total energies were studied further to determine any structural differences.

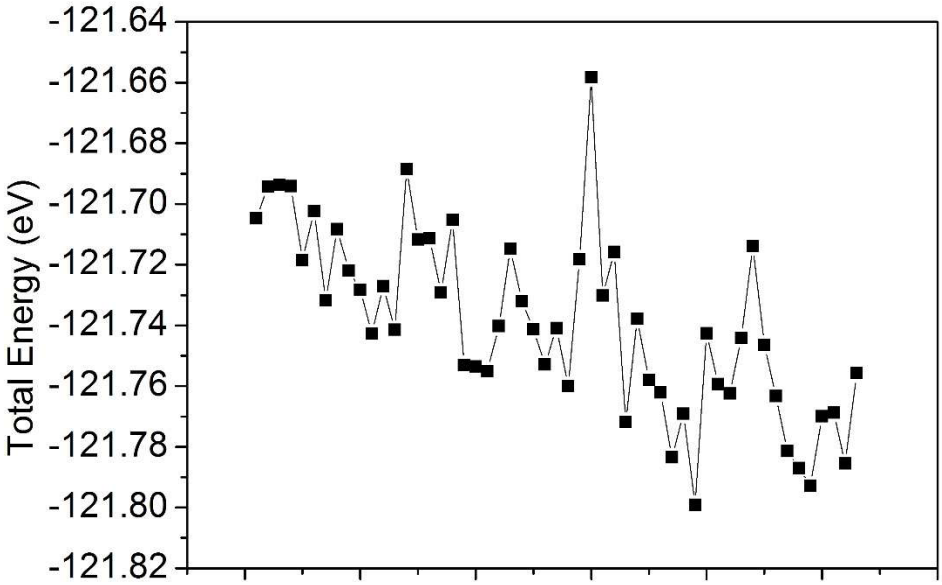

Figure 3-1: The variation in total energy of 53 unique configurations of non-stoichiometric palladium hydride ($PdH_{0.6875}$).

With an increased number of hydrogen vacancies, it was found that vacancies occurred in adjacent octahedral interstitial sites, creating vacancies “dimers”. Configurations with high total energy had two sets vacancy “dimers” (i.e. two hydrogen vacancy pairs), however no larger groups of nearest-neighbour vacancies were found. The lowest energy configuration was found to contain one vacancy “dimer” with the remaining vacancies spread throughout the cell. The highest and lowest energy configurations are shown in Figure 3-2.

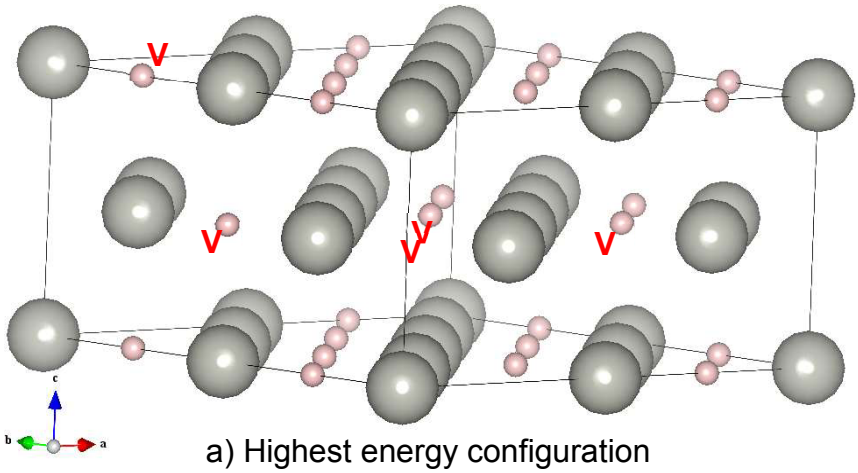

a) Highest energy configuration

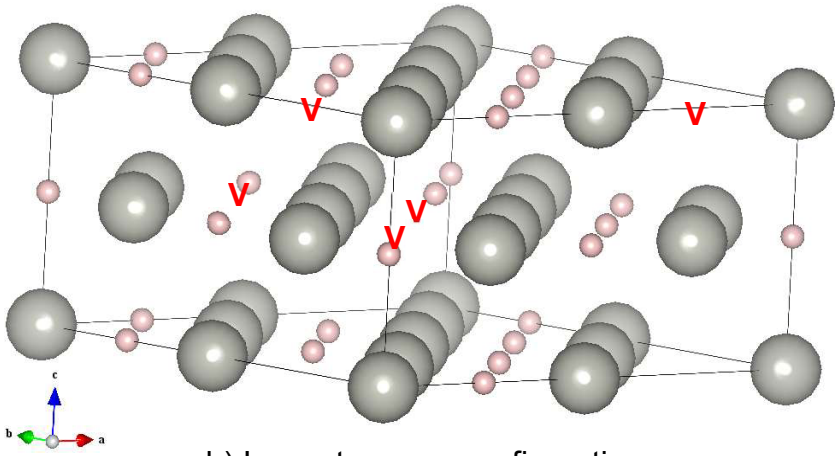

b) Lowest energy configuration

Figure 3-2: The highest (a) and lowest (b) energy configurations of $PdH_{0.6875}$, where palladium atoms are grey and hydrogen atoms are pink, showing that hydrogen vacancies in lower energy configurations are distributed throughout the material.

The energy of formation of PdH_x, where x = 0, 0.25, 0.5, 0.75 and 1, was studied, as shown in Table 3-4. This was achieved by modelling a 2x2x2 supercell of palladium metal with a 8x8x8 k-mesh. Hydrogen atoms were inserted into octahedral interstitial sites at random, until the desired molecular formula was achieved. The previous findings on hydrogen vacancy distribution was taken into account by spreading the hydrogen atoms throughout the cell.

Table 3-4: Change in energy of formation for palladium hydride (PdH_x) where x = 0, 0.25, 0.5, 0.75 and 1.

Molecular Formula	Total Energy (eV)	Energy of Formation ($\Delta_f H$) (eV)
Pd	-175.212	0.000
$PdH_{0.25}$	-203.299	-27.255
$PdH_{0.5}$	-232.169	-55.293
$PdH_{0.75}$	-260.605	-82.896
PdH	-288.351	-109.810

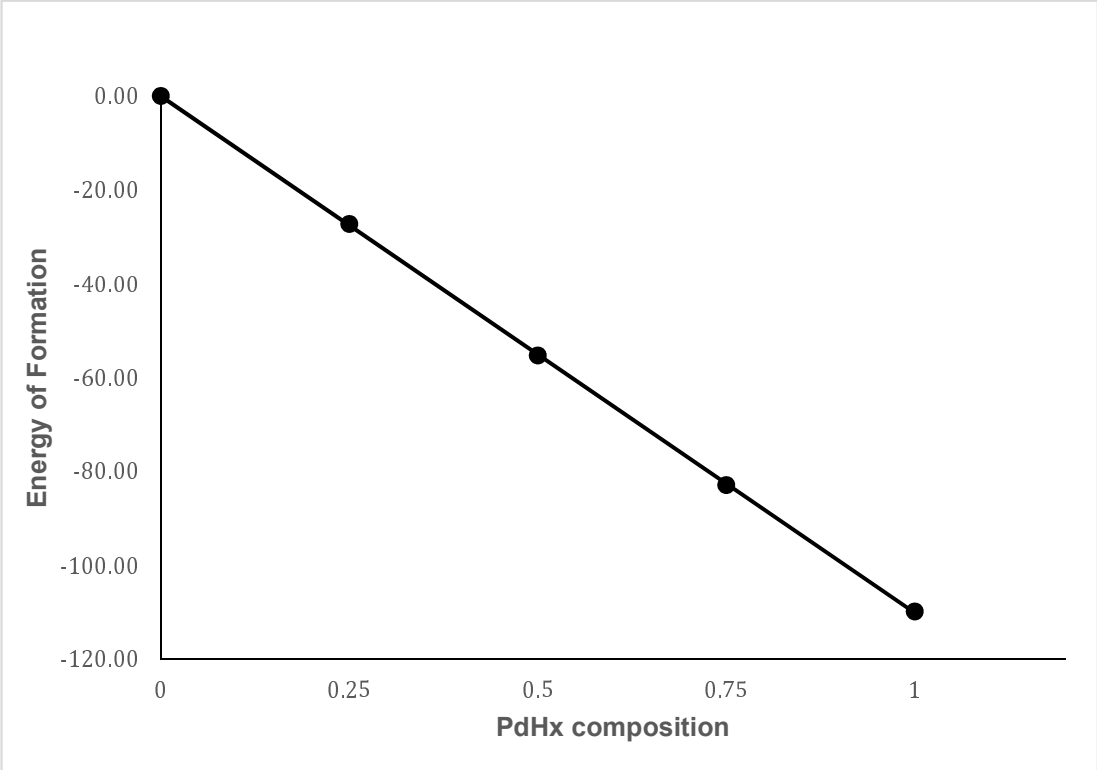

Figure 3-3: Change in energy of formation with increasing hydrogen content within palladium hydride

The energy of formation of PdH_x was found to decrease as the hydrogen content increased, suggesting that stoichiometric PdH is the most stable composition. However experimentally, it is difficult to achieve a molecular formula higher than $PdH_{0.7}$ without extremely high pressures.

3.3 Low Concentrations of Helium

The effect of distance between tritium and helium atoms on the cell length of palladium metal was studied by inserting a helium atom and a tritium atom into palladium metal at varying interatomic distances. All configurations contained 32 palladium atoms in an fcc structure with a helium atom placed in an octahedral interstitial site in the middle of the cell, whereas the tritium atom was placed in different octahedral sites with varying distances between the helium atom and tritium atom. The three systems were compared to a cell of palladium metal containing 32 palladium atoms, one helium atom and no tritium atoms. The total energy and cell length of each system was then compared to determine if the proximity of the tritium atom to the helium atom affects the stability of the material.

Table 3-5: The effect of helium – tritium distance on the cell length, crystal type and total energy of palladium metal, leading to slight lattice distortion.

Formula	No. of Tritium Atoms	No. of Helium Atoms	Helium – Tritium Distance (Å)	Cell Length (Å) (a = b)	Cell Length (Å) (c)	Crystal Type
Pd	0	0	-	7.9092	7.9092	cubic
$PdHe_{0.03125}$	0	1	-	7.9275	7.9275	cubic
$PdT_{0.03125}He_{0.03125}$	1	1	2.63	7.9849	7.9670	tetragonal
$PdT_{0.03125}He_{0.03125}$	1	1	4.85	7.9799	7.9727	tetragonal
$PdT_{0.03125}He_{0.03125}$	1	1	5.64	7.9808	7.9758	tetragonal

The cell parameter of the supercell containing one helium atom was found to be approximately 0.02 Å larger than that of palladium metal. This suggests that the introduction of helium leads to a slight expansion of the lattice in order to accommodate the additional atom. The palladium atoms adjacent to the helium atom have also moved away from their lattice sites in order to accommodate the larger volume of the helium atom compared to an interstitial vacancy.

The cell parameters of each of the three tritium configurations are approximately 0.05 Å larger than that of the $PdHe_{0.03125}$ system and approximately 0.08 Å larger than pure palladium metal. This implies that the lattice must expand again to accommodate the tritium atom, which has a larger volume than a vacancy. The tetragonal nature of each of the three configurations is only a very slight distortion from the cubic structure, where the cell parameter (c) in the Z direction is slightly shorter than the X and Y directions (cell parameters a and b). The small total energy differences between palladium metal and each of the compositions in Table 3-5 suggests that there is only a small difference in stability when adding one or two helium and tritium atoms. The distance between the helium and tritium atom does not largely affect the cell parameter or total energy of the system. This suggests that the tritium atom can occupy any vacant octahedral interstitial site with no effect on the stability of the system. When the helium and tritium atoms are 5.64 Å apart, there is only a 0.005 Å lattice distortion, suggesting that the atoms are at a sufficient distance to have little influence on each other.

DFT calculations discussed in Section 3.2, showed that despite the large number of possible configurations of PdT_x when tritium vacancies are introduced, each configuration has a very similar total energy, suggesting that the tritium atoms diffuse freely throughout the material and that any random configuration is likely to occur. It was also found in Section 3.2 that high-concentration tritium configurations with vacancies spread throughout the material exhibited the lowest total energy, compared to those with vacancies close together.

Three further 2x2x2 supercells of palladium tritide were constructed, as shown in Figure 3-4, with 32 palladium atoms in an fcc structure, one helium atom and an increasing concentration of tritium atoms. This series of calculations was performed in order to replicate the radioactive decay of a tritium atom into a helium-3 atom and the effect on neighbouring tritium atoms. The helium atom in each system was placed in an octahedral interstitial site in the middle of the cell, whereas the tritium atoms were placed in random octahedral sites spread throughout the cell.

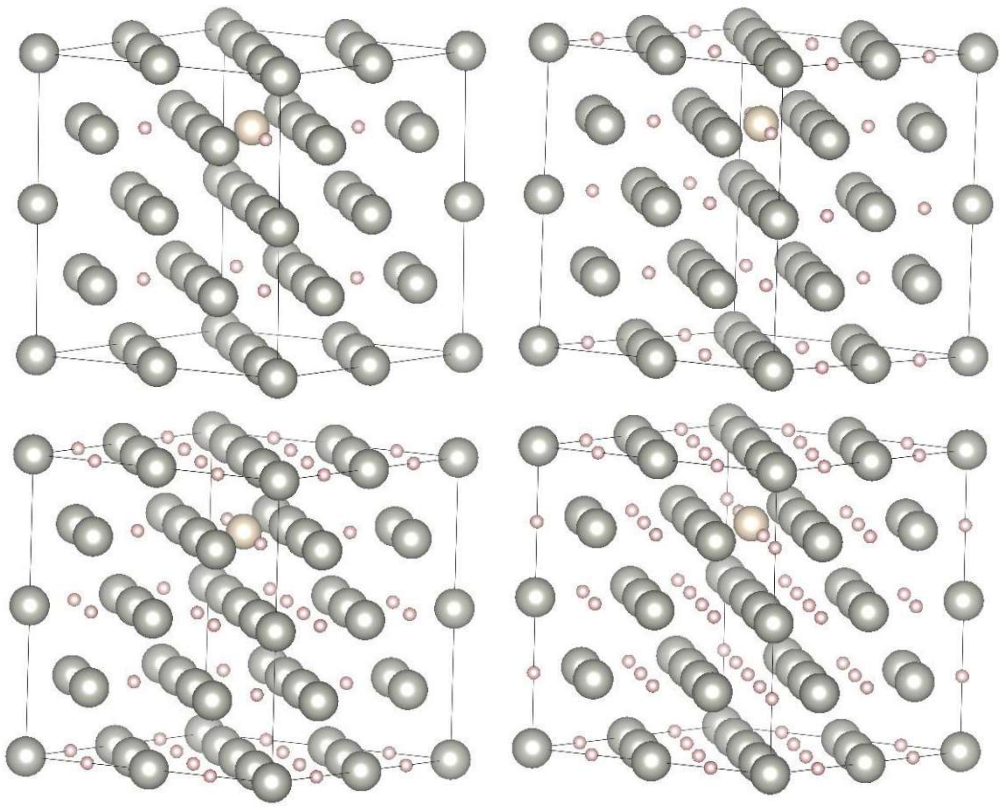

Figure 3-4: The composition of 25 % (top left), 50 % (top right), 75 % (bottom left) and 100 % (bottom right) occupied octahedral interstitial sites in palladium metal with one helium atom and increasing concentrations of tritium atoms.

The cell parameters of each system were compared with those for palladium metal with one helium atom and stoichiometric PdT with one helium atom, in order to investigate the stability of each system with respect to tritium concentration.

Table 3-6: The lattice distortion and change in formation energy of 2x2x2 supercells of palladium, with 25 %, 50 %, 75 % and 100 % occupied octahedral interstitial sites with increasing concentration of tritium atoms and one helium atom.

Formula	No. of Tritium Atoms	Occupied O_h Interstitial Sites (%)	Cell Length (Å) (a)	Cell Length (Å) (b)	Cell Length (Å) (c)	Crystal Type
Pd	0	0	7.9092	7.9092	7.9092	cubic
$PdHe_{0.03125}$	0	3.13	7.9275	7.9275	7.9275	cubic
$PdT_{0.21875}He_{0.03125}$	7	25	8.0739	8.0739	8.0266	tetragonal
$PdT_{0.46875}He_{0.03125}$	15	50	8.1835	8.1145	8.1514	orthorhombic
$PdT_{0.71875}He_{0.03125}$	23	75	8.2357	8.2357	8.2276	tetragonal
$PdT_{0.96875}He_{0.03125}$	31	100	8.3215	8.3215	8.3215	cubic

The addition of a helium atom into the palladium metal leads to a slight lattice expansion as described previously. When 25 % of the octahedral interstitial sites are occupied there is a lattice expansion of around 0.15 Å. The addition of the atoms also leads the cell to become distorted from cubic to a tetragonal

structure. The 50 % occupied system has a cell length that is about 0.11 Å larger than 25 % system and approximately 0.27 Å larger palladium metal. The 50 % occupied system was found to be the most distorted cell with an orthorhombic structure where each edge of the cell is of a different length, with the cell being longest in the a-direction. The cell length of the 75 % occupied system is approximately 0.04 Å larger than that of the 50 % system and around 0.33 Å larger than pure palladium. Finally, the system in which 100 % of octahedral interstitial sites are occupied, has a cell length which is approximately 0.1 Å larger than that of the 75 % system and about 0.41 Å larger than that of palladium metal. The change in cell length (a) with respect to the percentage of occupied octahedral interstitial sites, is shown in Figure 3-5.

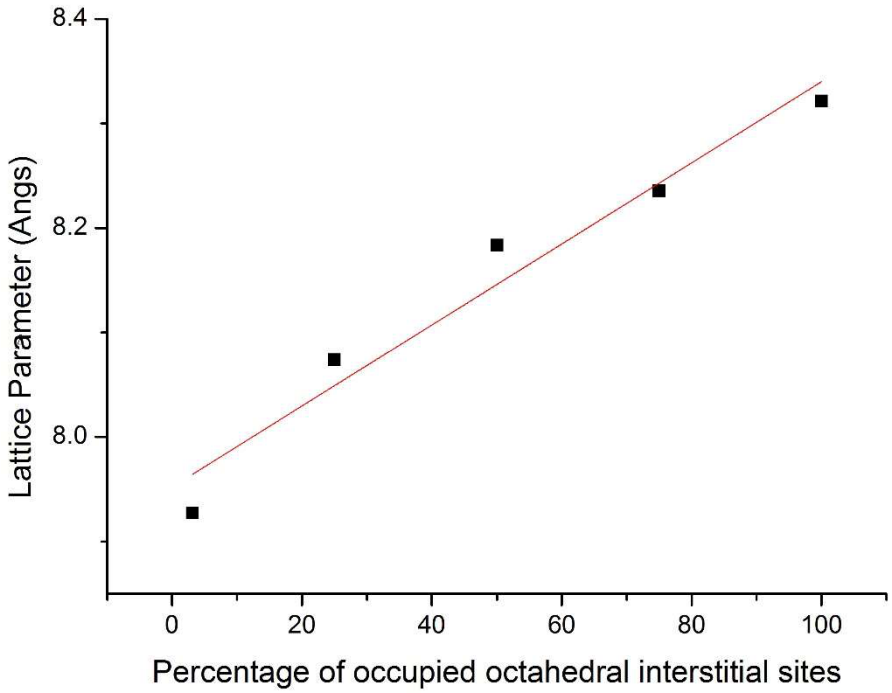

Figure 3-5: Change in cell length of a 2x2x2 palladium metal supercell with increasing percentage of octahedral interstitial site occupation by one helium atom and an increasing number of tritium atoms.

Figure 3-5 shows that as the number of occupied octahedral interstitial sites increases, the cell length of the supercell also increases almost linearly. The cell expansion can be attributed to the larger volume of a tritium atom compared with an unoccupied interstitial site. Additionally, as more tritium atoms are introduced, there is greater interaction between the atoms which may cause slight repulsion and lead to lattice expansion. It should be noted that there is only slight expansion between 50 and 75 % occupation, which corresponds with a phase transition of palladium tritide, where the material moves from the miscibility gap (a+b-phase) to the tritide phase (b-phase) of palladium tritide, where the phase transition occurs at T/Pd ~ 0.6. The slight reduction in expansion at 75 % occupation can also be attributed to a similar tritium content to that of the relatively stable $PdH_{0.7}$ formula. The extent of expansion increases between 75 and 100 % occupation which is expected as beyond $PdH_{0.7}$ it becomes more difficult to increase the hydrogen concentration, with fully occupied PdH only possible at extremely high pressures.

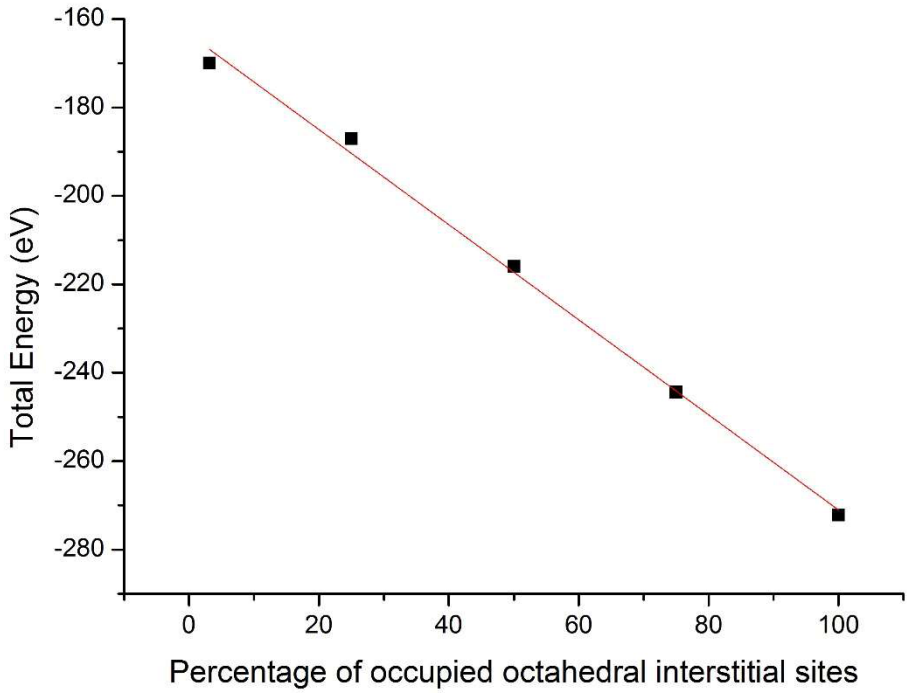

Figure 3-6: Change in total energy of 2x2x2 palladium supercell with increasing percentage of octahedral interstitial site occupation by one helium atom and an increasing number of tritium atoms.

Figure 3-6 shows the change in total energy with respect to percentage of occupied octahedral interstitial sites. It is shown that as the number of tritium atoms increases, the total energy of each system decreases almost linearly. This suggests that as the number of occupied octahedral interstitial sites increases the system becomes more exothermic and therefore more stable.

It is noteworthy that the total energy of the cell where 100 % of octahedral interstitial sites are occupied, is approximately 106 eV lower than that of palladium metal. The cell length of this configuration is also around 0.4 Å larger than that of palladium metal. However experimentally, it is expected that cells

with 75 % and 100 % occupation should be less exothermic and therefore less stable than cells with 50 % or less interstitial sites occupied, as compositions above T/Pd ~ 0.6 do not exist experimentally without extremely high pressures and temperatures.

Palladium metal and the 100 % occupied cell were found to be cubic, which is consistent with the cubic structure of palladium metal and experimental palladium tritide. Configurations with 25 % and 75 % occupation both have a tetragonal shape, where the cell parameter (c) in the Z-direction is approximately 0.05 Å shorter and 0.01 Å shorter respectively. An orthorhombic crystal shape is observed for the 50 % occupied system, where each cell parameter is a different length, with the cell parameter (b) in the Y direction being the shortest, whereas the cell parameter (a) in the X direction is approximately 0.07 Å longer. As the tritium atoms are randomly distributed throughout each cell, it can be expected that the distortion of the cell parameter may be different in each direction, as the cell must accommodate the relatively large tritium atoms in the smaller interstitial sites.

3.4 Helium Migration

The activation energy of the migration of a helium atom from one octahedral interstitial site to an adjacent octahedral interstitial site in PdT was calculated using nudged elastic band (Briec et al. 1986) theory. The Nudged Elastic Band method was achieved by geometry optimising initial and final configurations, under identical conditions, where the helium atom was situated in one of two adjacent vacant octahedral interstitial sites. These configurations replicated a

system in which a tritium atom had decayed to helium-3 and was able to use the decay energy to migrate to an adjacent vacant interstitial site. An intermediate configuration, or image, (approximated to be the transition state), where the helium atom was half-way between the two lattice sites was also created. Using NEB, the energy of the approximate transition state was calculated, leading to an estimation of the activation energy of the helium migration. In order to obtain a more accurate activation energy, an additional NEB calculation was performed with two intermediate configurations, in which the helium atom was one third and two thirds between the two lattice sites.

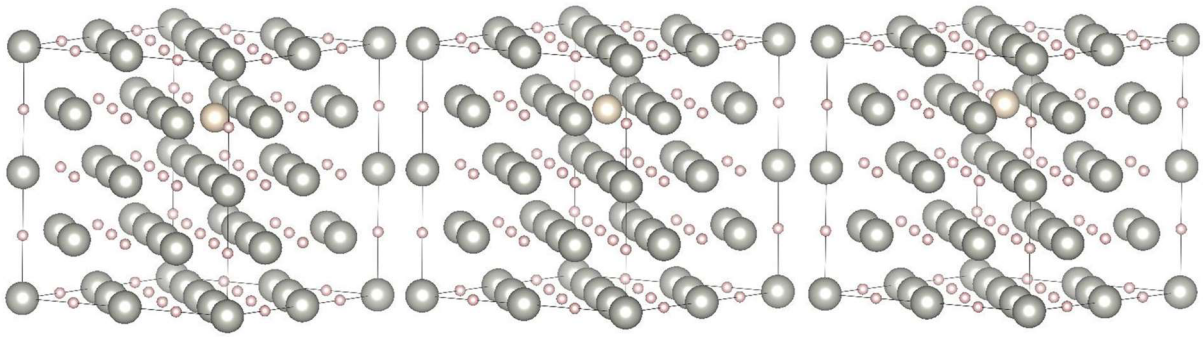

Figure 3-7: The migration of a helium atom between from an vacant octahedral interstitial site (left) via a transition step (middle) to an adjacent vacant octahedral interstitial site (right) in a 2x2x2 palladium tritide (PdT) supercell.

The activation energy of helium migration can be calculated by subtracting the total energy of the intermediate configuration from that of the initial or final configurations. The activation energy of the helium atom moving from the centre of the cell to the outer of the cell was found to be 1.419 eV. However, for the reverse direction the activation energy was found to be 1.423 eV. This

may have been caused by the distribution of tritide atoms compared to the helium atom and octahedral interstitial vacancies.

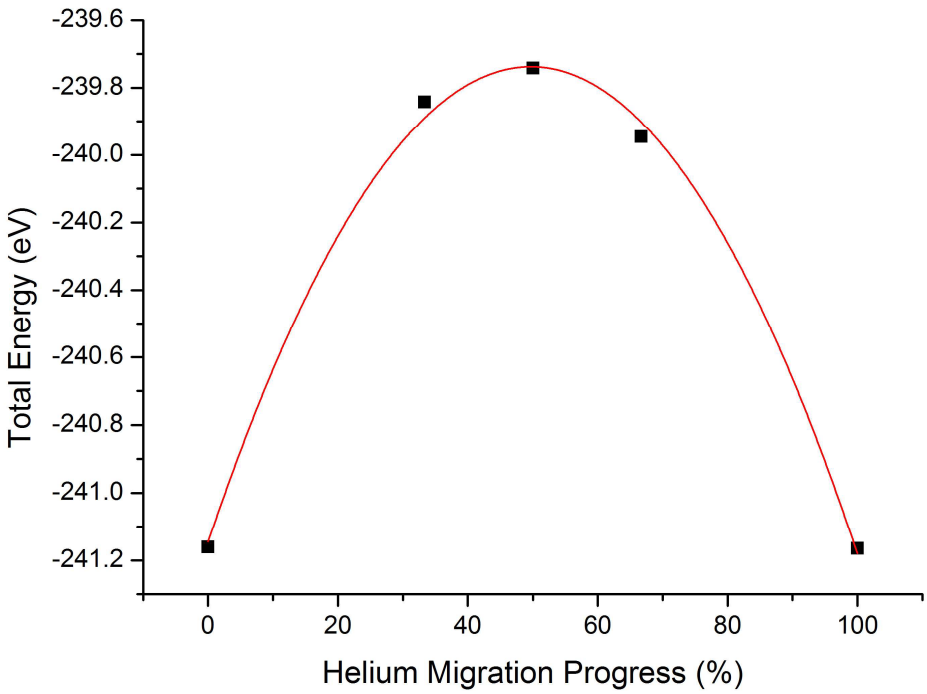

Figure 3-8: Change in total energy with helium migration between two octahedral interstitial sites.

Figure 3-8 shows the total energy differences between each configuration during the helium atom migration. As expected, the intermediate configuration has the highest total energy, suggesting that it is the least stable configuration. Additionally, this configuration was estimated to be the transition state of the helium migration.

Chapter 4

Interatomic Potential Derivation of Palladium Hydride

As a route to further exploring the thermodynamics of palladium tritide (PdT) and non-stoichiometric palladium tritide ($PdT_{0.65}$), molecular dynamics (MD) calculations were to be performed on the system. As a prerequisite, an accurate description, or forcefield, of the potential energy of the palladium-hydrogen system was required. To achieve this, a two-body interatomic potential known as a Buckingham potential (as shown in Equation 2-7) was used to describe short range hydrogen-hydrogen interactions and hydrogen-palladium interactions. Contributions from palladium-palladium interactions were omitted as the distance between the two ions (2.93 Å) was relatively large.

A cut-off radius of 20 Å was used in order to limit the inclusion of weak long-range interactions, which would make the calculation more computationally expensive.

In order to describe the atoms in the system, a rigid ion model and a shell model were compared to determine which model fitted better to *ab-initio* data.

In both models palladium metal was represented by a core only. In the rigid ion model the hydrogen atoms were also described by a core only. In the shell model, each hydrogen atom was represented by both a core and a shell.

Table 4-1 outlines the core charge on each palladium atom, as well as the core and shell charges on each hydrogen atom and the hydrogen spring constant.

Table 4-1: The core and shell charges and spring constant parameters used to represent palladium and hydrogen atoms in an palladium hydride (PdH) interatomic Buckingham potential, enabling the comparison of the rigid ion and core-shell modelling methods.

Model Method	Atom	Core Charge	Shell Charge	Spring Constant
Rigid ion	Palladium	+1.00	-	-
	Hydrogen	-1.00	-	-
Core-shell	Palladium	+1.00	-	-
	Hydrogen	+0.005	-1.005	4.24

Ultimately, a rigid ion model was used, as there was little difference in calculated parameters and it was found to be less computationally expensive than the core-shell model.

4.1 Stoichiometric Palladium Hydride

The lattice dynamics code General Utility Lattice Program (GULP 4.0.1) (Gale 1997) was used to fit the Buckingham potentials to reference lattice parameters, elastic constants and bulk modulus of PdH, which were previously calculated in this work using *ab-initio* finite differences energy minimization calculations.

Elastic constants define the properties of a material that undergoes stress, deforms, and then recovers and returns to its original shape. As palladium hydride is cubic, symmetry considerations meant that only C_{11}, C_{12} and C_{44} elastic constants were required to be calculated. The elastic constants of a unit cell of PdH were calculated by DFT finite differences method, with respect to ionic positions and lattice parameters. The bulk moduli of PdH was also calculated by determining the second derivative of a total energy curve with respect to cell volume.

A lithium hydride Buckingham potential (Pandey and Stoneham 1985, Haque and Islam 1992) was used as a starting point of the potential fitting due to the lack of a simple palladium hydride interatomic potential in the literature. Lithium hydride was selected for a number of reasons: both palladium and lithium hydrides have a 'rock salt' structure; lithium hydride has the formula LiH; and the lattice parameter of lithium hydride (4.062 Å) (Nolan, 2009) is similar to the lattice parameter of PdH calculated in this work (4.141 Å).

In order to accurately fit the palladium-hydrogen potential to the *ab-initio* data, the A and ρ values of the palladium-hydrogen Buckingham potential were manually changed before the least squares fitting procedure. Once suitable A and ρ values, which gave good fitting results, were determined, the palladium-hydrogen Buckingham potential was fitted further by allowing GULP to automatically fit A and ρ. Static structural and energy optimisations were performed under constant pressure to determine the relaxed structure of a unitcell of PdH.

Table 4-2: Parameters of interatomic Buckingham potentials for Pd – H and H – H interactions in palladium hydride (PdH), fitted against ab-initio DFT calculations, as determined in this work.

	Ion Pair	A (eV)	Rho (Å)	C (eVÅ^6)	Atomic Charge (e)	
PdH	Pd – H	4049.856	0.210	0.000	Pd	+1.00
	H – H	6611.249	0.132	0.980	H	-1.00

Table 4-2 shows the fitted values for A, Rho and C of palladium – hydrogen and hydrogen – hydrogen Buckingham potentials for stoichiometric palladium hydride.

Table 4-3: Lattice parameters and elastic properties of palladium hydride (PdH) determined using interatomic Buckingham potentials compared to ab-initio calculations, as determined in this work.

Property	Fitted Potential	*Ab-initio* DFT	% error
Lattice Constant (Å)	4.144	4.141	0.06
C11 (GPa)	201.7	193.5	4.20
C12 (GPa)	43.5	165.6	73.71
C44 (GPa)	58.0	57.5	0.87
Bulk Modulus (GPa)	96.3	75.0	28.33

Table 4-3 shows the percentage error of fitting for PdH Buckingham potentials compared to DFT calculations also calculated in this work. The potentials for PdH compared extremely well with DFT lattice constants and C_{11} and C_{44} elastic constants, with percentage errors of 0.06, 4.20 and 0.87 respectively. However, the C_{12} elastic constant fitted less well, as it had a percentage error of 73.71. This discrepancy can be explained by the Cauchy relation, where $C_{12} = C_{44}$, However "rock salt" structure materials, including palladium hydride, violate the Cauchy relation and therefore $C_{12} \neq C_{44}$ as shown by experimental results (Nygren and Leisure 1988) and DFT calculations from this work. However, when fitting the potentials, this violation was not taken into account and therefore C_{12} and C_{44} were found to be similar values for the interatomic

potential. This led to a fairly large percentage error deviation in the bulk modulus, which is dependent on C_{12}.

4.2 Non-Stoichiometric Palladium Hydride

The Buckingham potentials for PdH were subsequently used as a starting point to derive the potentials for $PdH_{0.75}$. This non-stoichiometric formula was selected as it was similar to the experimental formula of $PdH_{0.7}$ and only one hydrogen atom was required to be removed from the unit cell. This was achieved by modifying the occupancy of the hydrogen atoms to 0.75 instead of 1.0 and reducing the charge on each palladium atom from +1.00 to +0.75.

Initially, the non-stoichiometric palladium hydride Buckingham potential was to be fitted to *ab-initio* calculations of elastic constants derived in this work. However, it was found that *ab-initio* energy minimisation calculations of non-stoichiometric palladium hydride did not converge. Therefore the $PdH_{0.75}$ Buckingham potential was fitted to work in the literature, where the lattice constant was fitted to *ab-initio* work by Zhou *et al. (Zhou et al. 2008)* and elastic properties were fitted to experimental work by Nygren and Leisure*. (Nygren and Leisure 1988)*. The constants calculated in this work were compared with experimental results (Schwarz et al. 2005).

Table 4-4: Parameters of interatomic Buckingham potentials for Pd – H and H – H interactions in non-stoichiometric palladium hydride ($PdH_{0.75}$), fitted against experimental data *(Nygren and Leisure 1988)*.

	Ion Pair	A (eV)	Rho (Å)	C (eVÅ^6)	Atomic Charge (e)	
$PdH_{0.75}$	Pd – H	7049.856	0.210	32.675	Pd	+0.75
	H – H	372952470	0.126	0.980	H	-1.00

Table 4-4 shows the fitted values for A, Rho and C of palladium – hydrogen and hydrogen – hydrogen Buckingham potentials for non-stoichiometric palladium hydride. The fitting of the $PdH_{0.75}$ potential was influenced by a significant change in A for the H – H interaction and a large change in C for the Pd – H interaction.

The lattice constant, C11 and C44 obtained from the $PdH_{0.75}$ potentials fitted well to experiment, with percentage errors of 0.00, 12.07 and 4.12 respectively, as shown in Table 4-4 which shows the fitted values for A, Rho and C of palladium – hydrogen and hydrogen – hydrogen Buckingham potentials for non-stoichiometric palladium hydride. The fitting of the $PdH_{0.75}$ potential was influenced by a significant change in A for the H – H interaction and a large change in C for the Pd – H interaction.

Table 4-5: Lattice parameters and elastic properties of non-stoichiometric palladium hydride ($PdH_{0.75}$) determined using interatomic Buckingham potentials compared to experimental data (Nygren and Leisure 1988).

Property	Fitted Potential	Experiment (Nygren and Leisure 1988)	% error
Lattice Constant (Å)	4.109	4.109	0.00
C11 (GPa)	251.5	224.4	12.07
C12 (GPa)	67.5	162.0	58.33
C44 (GPa)	67.5	64.8	4.12
Bulk Modulus (GPa)	128.8	183.0	29.61

Table 4-5 shows that, as with PdH, C12 did not fit well with experiment due to the violation of the Cauchy relation. The fitted bulk modulus was 29.61 percent smaller than experiment, as expected due to a dependency on the C12 elastic constant.

Chapter 5

Surfaces of Stoichiometric and Non-Stoichiometric Palladium Hydride

5.1 Introduction

The common surfaces of cubic palladium hydride are the {100}, {101} and {111} surfaces. The energetics and structure of these surfaces is explored in this Chapter. To date, very little research has been reported on the surfaces of palladium hydride or tritide, especially comparing all three surfaces. It is possible that this work is the first to study all three surfaces within the same body of work.

In order to cut surfaces from the bulk atomistic simulation, the Metadise code (Watson et al. 1996) was used. Each surface consisted of region 1 and region 2 areas. The atoms in region 1 were those nearest to the surface and were allowed to fully relax. The atoms in region 2 were kept fixed, further from the surface, representing the bulk material. The final configuration of each surface was relaxed by performing static conjugate gradient and Newton-Raphson energy minimisation calculations using the interatomic potentials derived in Chapter 4.

Jigato *et al.* used Density Functional Theory to calculate the interplanar distances between each layer of the H-terminated and Pd-terminated {111} surface of stoichiometric palladium hydride (Jigato et al. 2003). The {111} surface was studied due to its use as a catalyst in the hydrogenation process. It was found that surface effects are visible until the 5^{th} layer of the material. Additionally, the Pd-terminated surface is found to have a lower surface energy than that of the H-terminated surface.

5.2 Stoichiometric Palladium Hydride

Planar surfaces of PdH were cut from the bulk material using the Metadise code (Watson et al. 1996) and the Buckingham potential developed previously. Four different surfaces were cut; {100}, {101}, faceted {101} and {111}. Figure 5-1 shows each of the relaxed PdH surfaces in the x-z and x-y planes. The {100} and planar {101} surfaces had two different terminating surfaces, where the palladium and hydrogen atoms were alternated. The {111} surface had a Pd-terminated and H-terminated surface. It was found that each surface energy was the same for different terminations. After relaxation, each surface showed very little distortion compared to the unrelaxed structure.

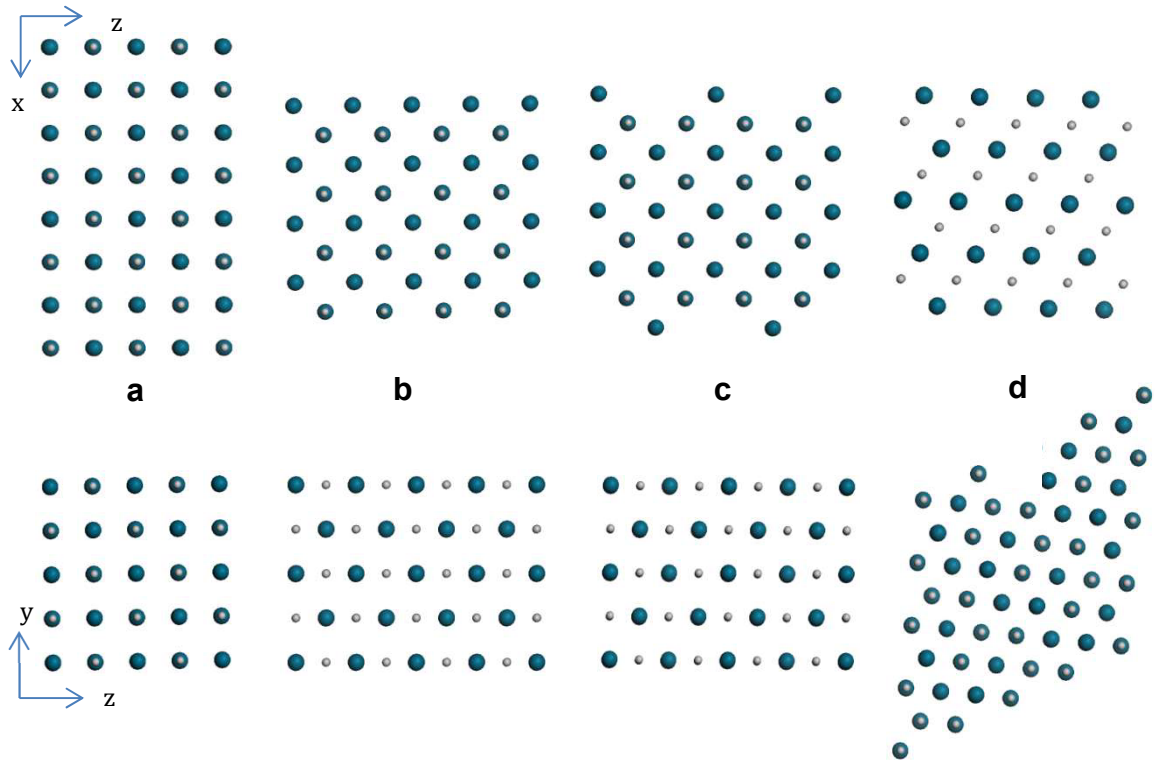

Figure 5-1: Common surfaces of palladium hydride (PdH) after the relaxation of atoms, viewed from the side (upper images) and top (lower images) orientations, where a is the {100} surface, b is the planar {101} surface, c is the faceted {101} surface and d is the palladium-terminated {111} surface.

The surface energy of each planar surface was calculated, as shown in Table 5-1, using the following equation:

Equation 5-1: Total Surface Energy

$$\text{Total Surface Energy} = \frac{E_{Slab} - E_{Bulk}}{A}$$

Where U_S is the energy of the cut surface, U_B is the energy of the bulk and A is the surface area of the cut surface.

Table 5-1: A comparison of lattice distortion, total surface energies and average atomic inter-planar distance for {100}, faceted {101}, planar {101} and {111} surfaces of palladium hydride (PdH).

Surface	Cell Type	Total Surface Energy ($J\ m^{-2}$)	Average inter-planar distance (Å)	
			This Work	Ab-initio DFT (Jigato et al. 2003)
Bulk PdH	cubic	-	2.072	-
{100}	cubic	0.469	2.071	-
Faceted {101}	cubic	1.141	1.457	-
Planar {101}	cubic	1.511	1.454	-
{111} Pd-Terminated	monoclinic	1.690	1.175	1.173
{111} H-Terminated	monoclinic	1.691	1.176	1.155

Both the {100} and {101} surfaces of PdH were cubic, whereas the {111} surface was found to be monoclinic. The {101} surface of PdH had two different terminating surfaces, one planar and one faceted, where two rows of palladium

and hydrogen atoms are transposed from the top of the surface to the bottom of the surface.

The most energetically favourable surface of PdH, as shown in Table 5-1 was found to be the {100} surface. The {100} surface of PdH was found to have the same structure as the bulk material. The {111} surface was found to be the least stable surface. The faceted {101} surface energy was 0.37 J m^{-2} lower than planar {101} surface, suggesting that the faceted {101} is more energetically favourable.

Average inter-planar distances of each relaxed surface in the z-direction were calculated. It was found that the {100} surface inter-planar distance was 0.001 Å less than that of bulk palladium hydride, which is to be expected as the surface is the same as the bulk material. The inter-planar distance {101} surfaces is approximately 0.615 Å smaller than the bulk material. The planar {101} surface and the faceted {101} surface have very similar inter-planar distances, with a difference of 0.003 Å. This suggests that the faceted nature of the surface has little effect on the inter-planar distance. It was found that surfaces with a smaller inter-planar distance had a larger total surface energy. This trend may be caused by the atoms interacting as they become closer together.

{111} PdH surfaces from this work were compared to those produced by Jigato *et al.* (Jigato et al. 2003), whereas no existing research on the properties of {100} and {101} surfaces of PdH was found. The {111} surface was also

selected as it was found to readily undergo hydrogen absorption (Okuyama et al. 1998).

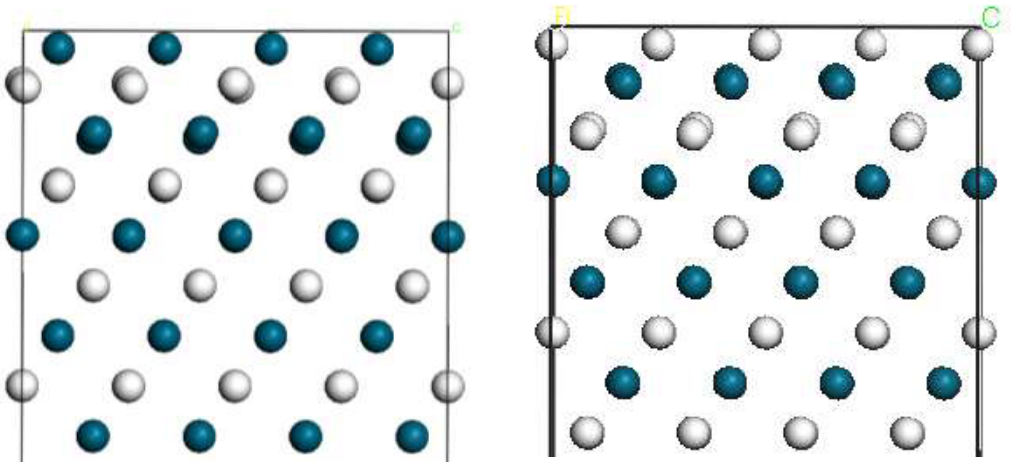

Pd-Terminated H-Terminated

Figure 5-2: Palladium (left) and hydrogen (right) terminated surfaces of the {111} surface of palladium hydride (PdH), as viewed from the side orientation.

The average distance between adjacent surface layers (inter-planar distance) for the {111} surface in this work (1.175 Å) compared well to the average distance of 1.173 Å found by Jigato *et al*. The average inter-planar distances of {111} Pd- and H-terminated surfaces calculated in this work were found to be more consistent with each other, as the difference was 0.001 Å compared to 0.018 Å for Jigato et al (Jigat et al. 2003).

In this work, the inter-planar distance for the {100} surface converged to 0.001 Å after the 3rd layer of atoms, with all other surfaces converging after the 4th layer. The inter-planar distance of the {100} surface was very similar to that of the bulk PdH, which is not unexpected, as the structure is the same for both materials.

{111} surfaces constructed in this work were compared to those studied by Jigato *et al*. as shown in Table 5-2 (Jigato et al. 2003). The inter-planar distances of the {111} surfaces studied by Jigato *et al.* only converged to 0.1 Å after 13 surface layers, compared with this work where the inter-planar distance converged to 0.001 Å after the 4^{th} surface layer. This suggests that the surface effects in this work are less pronounced and have less of an effect on the lower layers of the material. Jigato et al. observed a large difference between the inter-planar distances of hydrogen and palladium-terminated {111} surfaces, whereas this work determined that the interplanar distances were very similar for both terminating variety of surface. Jigato *et al.* also suggested that the palladium-terminated {111} surface was less stable than the hydrogen-terminated surface, whereas this work has found that the palladium-terminated surface is slightly more stable, with a very small total surface energy difference of 0.0003 J m^{-2}. This suggests that the interatomic potential derived in this work, treats the two terminating surfaces similarly.

Table 5-2: The distance between adjacent surface layers (interplanar distance) of palladium and hydrogen-terminated {111} surfaces of palladium hydride (PdH) compared to equivalent distances calculated in the literature (Jigato, Coussens et al. 2003)

Interplanar Distances of {111} Hydrogen-Terminated Surface (Å)		Interplanar Distances of {111} Palladium-Terminated Surface (Å)	
This Work	**(Jigato, Coussens et al. 2003)**	**This Work**	**(Jigato, et al. 2003)**
0.877	0.800	0.879	0.678
1.190	0.997	1.190	1.683
1.200	1.441	1.200	0.975
1.197	1.021	1.197	1.356
1.196	1.338	1.196	1.086
1.196	1.082	1.196	1.258
1.196	1.272	1.196	1.136

5.3 Non-Stoichiometric Palladium Hydride

The surfaces of $PdH_{0.75}$ had the same structure as those for PdH, although 25 percent of hydrogen atoms were removed, leaving hydrogen vacancies. The unrelaxed and relaxed structures of {100}, {101} and {111} surfaces of $PdH_{0.75}$ are shown in Figure 5-3.

As discussed in Chapter 3, the vacancies were spread throughout the material for all surfaces. However to reduce the surface dipole to a minimum, two hydrogen atoms were removed from each layer in the z-direction, allowing the vacancies to be a sufficient distance apart in each direction. In order to minimise the surface dipole as much as possible, the vacancies were created in an alternating pattern in each inter-atomic layer, as shown in Figure 5-4. However, this meant that there were hydrogen vacancies both above and below certain palladium atoms, leading to these atoms moving from their atom site after relaxation. The Buckingham interatomic potentials for $PdH_{0.75}$, as derived in Chapter 4, were used to model the surfaces.

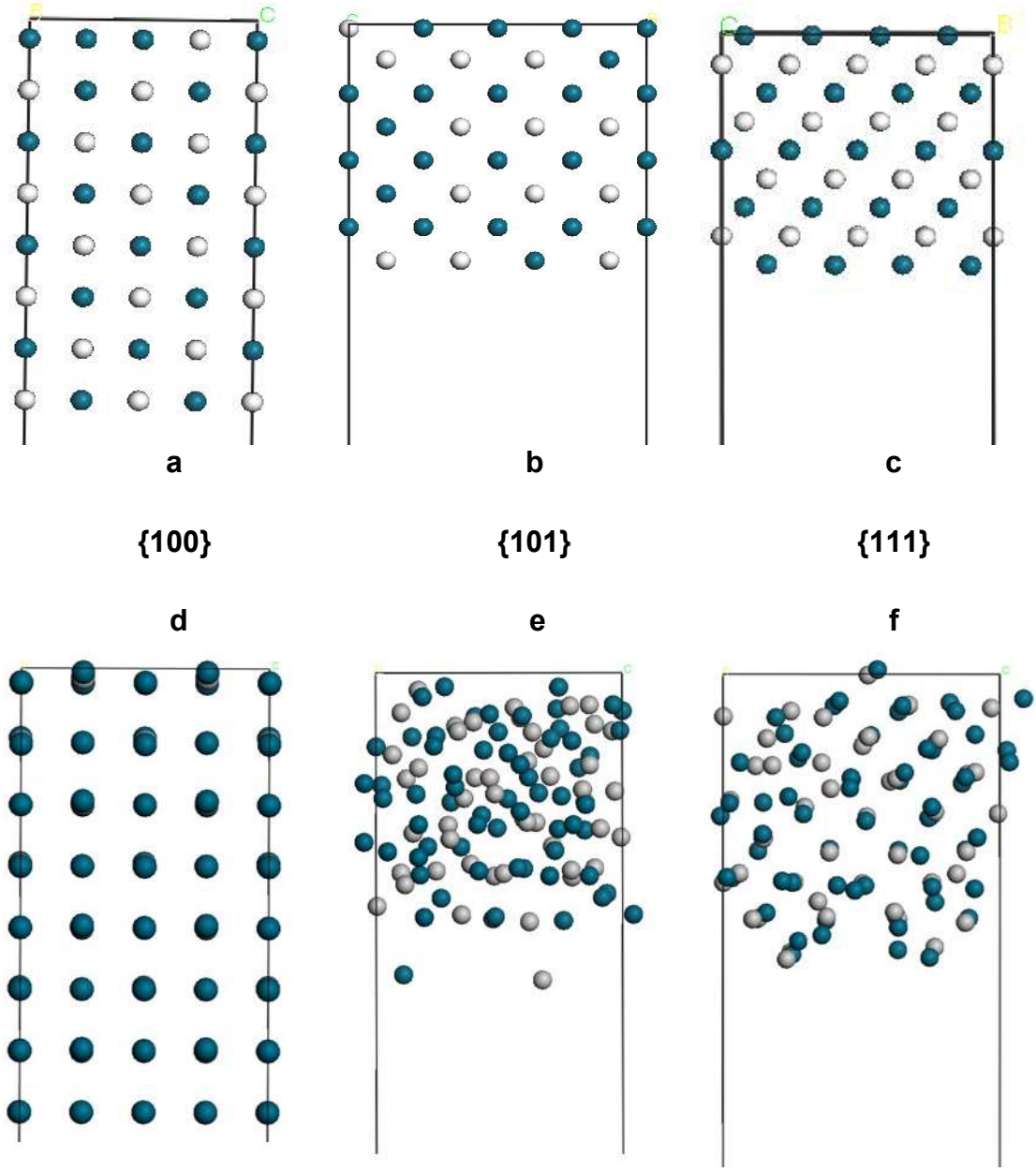

Figure 5-3: Side view orientations of the common surfaces of non-stoichiometric palladium hydride ($PdH_{0.75}$), including the {100} surface prior to (a) and post (d) relaxation, {101} surface prior to (b) and post (e) relaxation and palladium-terminated {111} surface prior to (c) and post (f) relaxation.

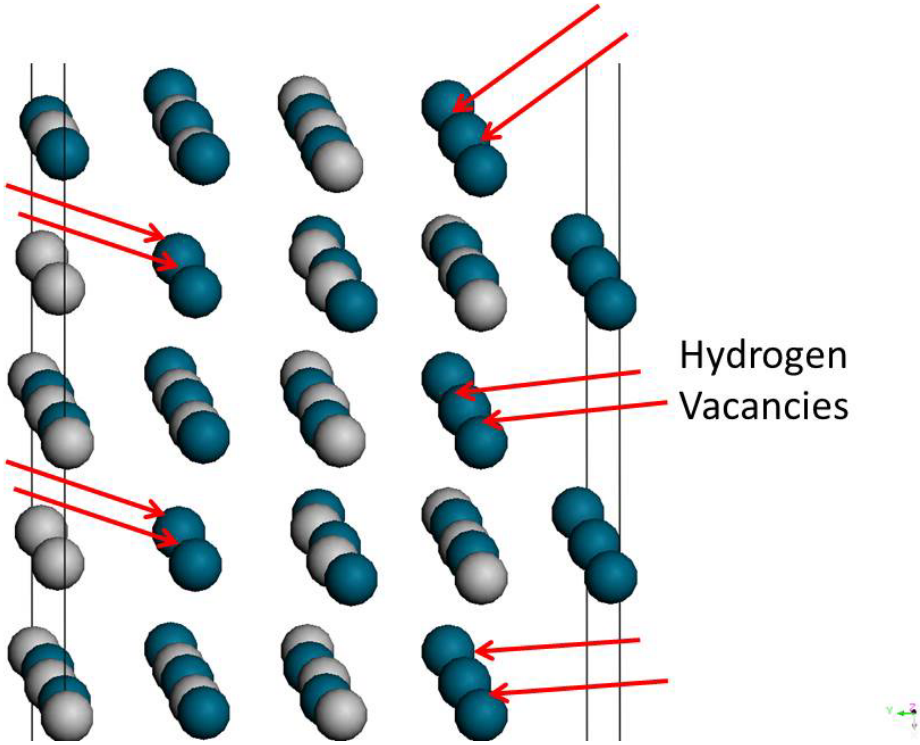

Figure 5-4: A side view orientation of the unrelaxed {100} surface of non-stoichiometric palladium hydride ($PdH_{0.75}$) with two hydrogen octahedral interstitial vacancies per surface layer, where palladium atoms are blue and hydrogen atoms are white.

The configurations studied in this work were those which produced a small initial surface dipole between -0.005 and zero. Other possible configurations may lead to more or less stable surfaces, however due to time constraints the vacancies were positioned on a “trial and error” basis until a sufficiently small surface dipole was found. It would be possible to use the Site Ordered Deficiency (SOD) code (Grau-Crespo et al. 2007), as discussed in Chapter 3 to determine each possible configuration, although calculating the surface dipole and surface energy for each configuration would be time intensive.

The removal of hydrogen atoms led to destabilisation of each surface where, after relaxation, physical distortion occurred close to the surface and some atoms moved from initial atomic sites, as shown in Figure 5-3.

The {100} surface showed only slight distortion, with little or no movement of atoms from their atomic sites. This suggests that the {100} is relatively stable, a finding which is further supported by the low surface energy compared to other $PdH_{0.75}$ surfaces. Figure 5-5 shows the distances between selected atoms in the {100} surface. The palladium – hydrogen distance for the PdH {100} surface and bulk PdH was 2.072 Å, however the same distance in the $PdH_{0.75}$ {100} surface was found to be 2.062 Å. This suggests that the atoms have moved slightly from their atomic sites to counteract the hydrogen vacancies within the material. Additionally, the palladium – palladium distance was measured where a hydrogen vacancy existed between the two atoms. For the $PdH_{0.75}$ {100} surface, the Pd-Pd distance was 4.253 Å, compared with 4.144 Å for the PdH {100} surface. However, this distance was measured close the surface, between the 1st and 3rd atomic layers, rather than deeper into the surface and therefore surface effects may have caused the distance to be larger than average. A palladium – palladium distance of 4.124 Å was found between the 7th and 9th layers, which is more comparable to the PdH {100} palladium – palladium distance. This suggests that further from the surface, the $PdH_{0.75}$ {100} surface is very similar to {100} PdH and bulk PdH, with little distortion caused by the hydrogen vacancies.

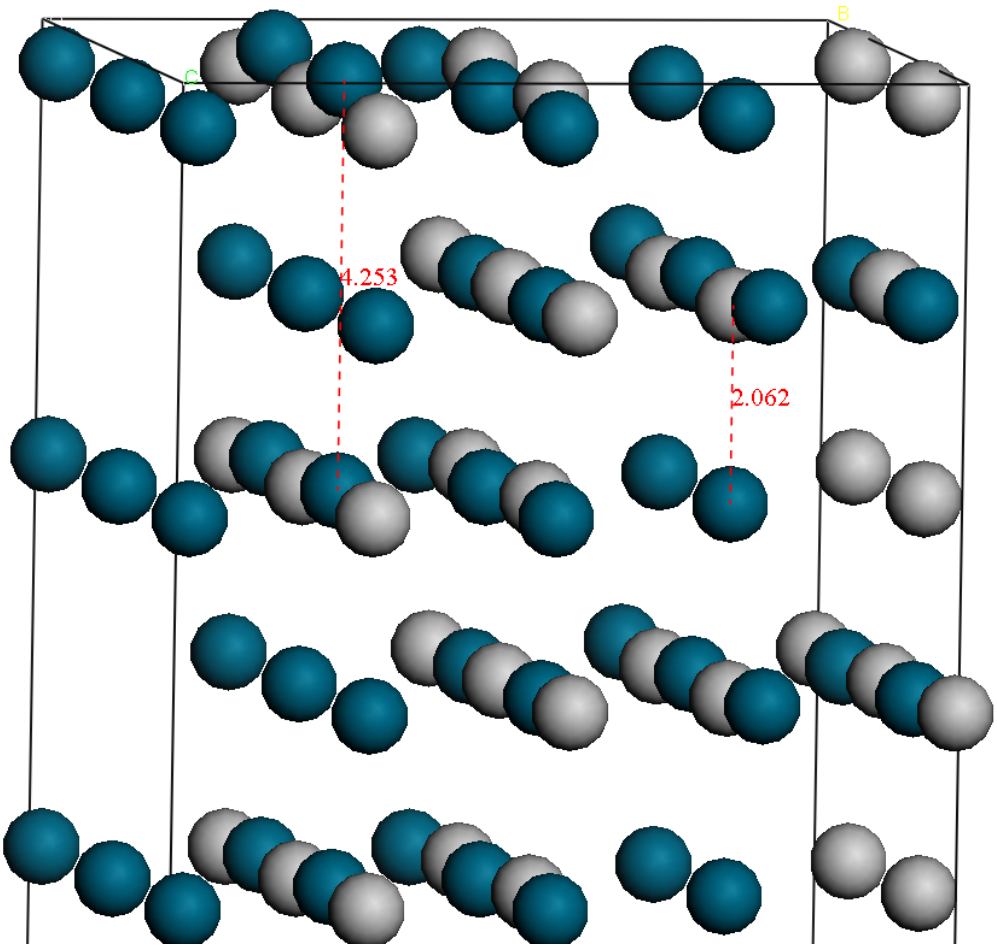

Figure 5-5: A side view orientation of the relaxed {100} non-stoichiometric ($PdH_{0.75}$) surface, indicating movement of atoms and distance between surface layers due to two hydrogen vacancies per surface layer.

Both the {101} and {111} surfaces showed significant distortion, as shown in Figure 5-2, where the majority of atoms moved from their atomic sites. This was most likely caused by the destabilising effect of introducing hydrogen vacancies, as the surrounding atoms attempt to rearrange to accommodate the holes in the material. This finding also explains the significant increase in

surface energy compared with the {100} surface, where planar {101} has an energy difference of 0.243 J m^{-2} and the {111} surface has an energy difference of 0.332 J m^{-2}.

Table 5-3 – A comparison of the total surface energies of the {100}, {101} and {111} surfaces of non-stoichiometric palladium hydride ($PdH_{0.75}$).

Miller Index Surface	Total Surface Energy (J m^{-2}) $PdH_{0.75}$	Total Surface Energy (J m^{-2}) PdH
{100}	0.483	0.469
Faceted {101}	0.555	1.141
Planar {101}	0.726	1.511
{111}	0.815	1.690

The $PdH_{0.75}$ surfaces follow the same energy trend as the PdH surfaces, as can be seen in Table 5-3, with the {100} surface the most energetically stable and the {111} surface the least energetically stable. The surface energy of the {111} surface is almost double that of the {100} surface.

All surfaces, except the {100} surface, have a lower total surface energy than the corresponding PdH surface. This suggests that the $PdH_{0.75}$ systems are more energetically stable than the PdH systems, which is expected as $PdH_{0.75}$ is closer to the experimental composition of $PdT_{0.65}$. However, the physical

distortion observed for the {101} and {111} in Figure 5-2 suggests that the $PdH_{0.75}$ surfaces are less stable than the equivalent PdH surfaces.

The total surface energy of $PdH_{0.75}$ {100} surface is slightly higher than that of the PdH surface, however the two surfaces are very close in energy (ΔE = 0.014 J m^{-2}). This difference may be due to two hydrogen vacancies on the terminating surface, leading to slight destabilisation of the surface.

Stepped surfaces of the PdH {100} surface were subsequently cut to be used as a grain boundary of palladium hydride for Molecular Dynamics simulation, as discussed in Chapter 6.

Chapter 6

Molecular Dynamics Simulations of Palladium Hydride Grain Boundaries

6.1 Bulk Palladium Hydride

Using the fitted PdH Buckingham potentials from this work, a molecular dynamics simulation of a 5x5x5 supercell of bulk PdH, containing 500 palladium atoms and 500 hydrogen atoms, was performed using DL_POLY 2.20 (Smith, 2006, Todorov, 2006). The temperature and pressure of the system were fixed at 300 K and 1 bar respectively and a 0.005 ps timestep was used. The system was equilibrated by running NVE, NVT-hoover and NVP-hoover ensembles in succession for 1 ns each. The final configuration of the system for each ensemble was used as a starting point for the subsequent ensemble. The production run of the simulation was carried out for 4.5 ns using the NPT-hoover ensemble. The system was fully relaxed after 7.5 ns when configurational energy had converged with respect to simulation time.

The energy convergence of the system suggests that the Buckingham potentials derived in this work are stable and suitable for modelling bulk PdH. This statement is additionally supported by the observation of no change in

lattice constant and atoms remaining situated on their lattice sites after relaxation of the material.

Figure 6-1 shows the relaxed structure after 7.5 ns of atomistic simulation. The lattice parameter of the relaxed structure was found to be 4.144 Å and the palladium – hydrogen interatomic distance was 2.072 Å, compared to a lattice parameter of 4.141 Å as calculated by Density Functional Theory, which is discussed in Chapter 3 of this work and experimental $PdH_{0.7}$ (4.040 Å) (Maeland and Flanagan 1966).

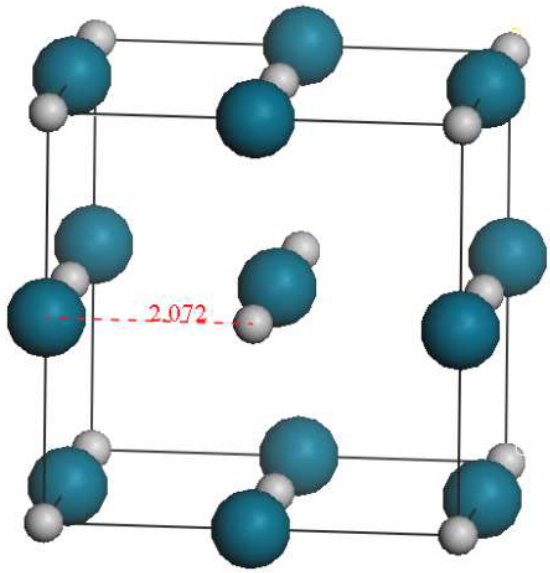

Figure 6-1: A snapshot of the relaxed atomistic simulation of bulk palladium hydride (PdH) after 7.5 ns, indicating distance in Angstroms between palladium and hydrogen atoms.

6.2 Grain Boundaries of Palladium Hydride

Using the stepped surfaces as discussed in Chapter 5, a grain boundary was constructed using the Metadise code (Watson et al. 1996). Subsequently a Molecular Dynamics (MD) simulation was performed for each grain boundary.

6.2.1 Stoichiometric Palladium Hydride

The {100} stepped surface of PdH was used as a starting point to create a palladium hydride grain boundary as this surface was found to be the most energically stable, as discussed in Chapter 5. The stepped surface was reflected, with a sufficient distance between the two surfaces to interact but not too close that the surfaces touched. This was achieved by modifying the distance between the two surfaces until a distance of 2.950 Å at the closest point and 9.534 Å at the furthest point was achieved as shown in Figure 6-2.

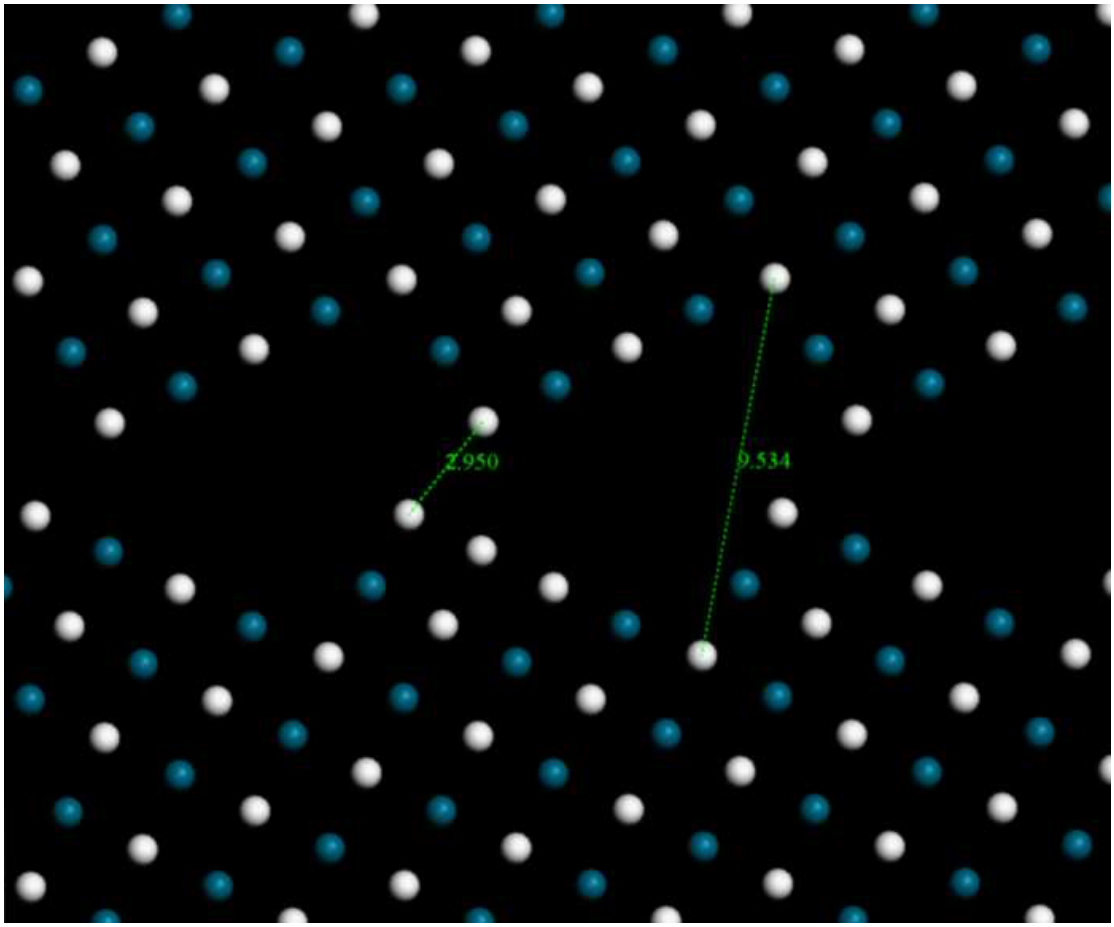

Figure 6-2: A side view of the orientation of two stepped {100} PdH surfaces prior to molecular dynamics simulation. A grain boundary is created between the two surfaces, with indication of the largest and shortest distance between the two surfaces in Angstroms.

The atomic coordinates, along with the earlier developed potential, were inputted into the DLPOLY 2.20 code (Smith, 2006, Todorov, 2006), using the same variables as discussed for bulk palladium hydride in Section 6.1. In total, there were 1152 palladium atoms and 1152 hydrogen atoms. The system was equilibrated for 40 ps with a timestep of 0.005 ps using the NVE ensemble followed by NVT-hoover and finally NPT-hoover. A production run was then

performed, consisting of 200 ps NPT-hoover. In total, 240 ps of simulation was carried out until the total energy of the system had converged.

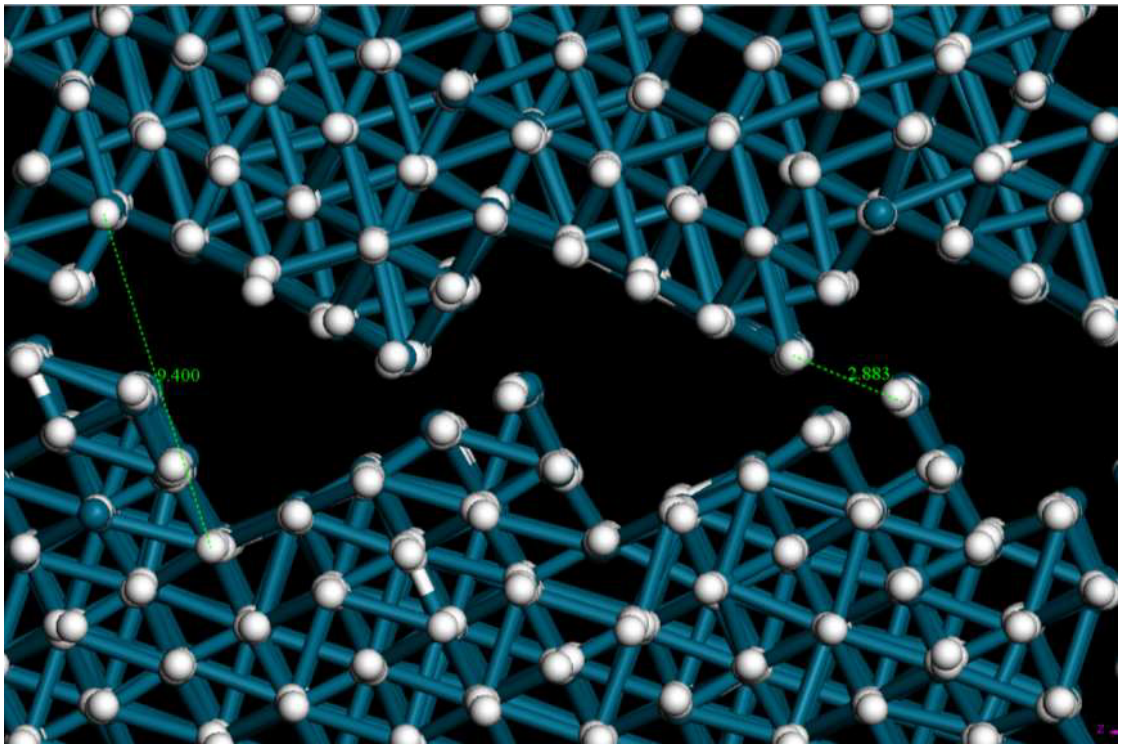

Figure 6-3: A side view of the relaxed grain boundary structure of PdH after 240ps simulation, showing that the surfaces have moved slightly closer together, whilst the grain boundary remains intact.

The relaxed grain boundary is shown in Figure 6-3. It was found that the distance between the two surfaces had decreased to 9.400 Å at the furthest distance and 2.883 Å at the closest part, a reduction of 0.134 Å and 0.067 Å respectively. The minimal change in distance after relaxation is promising, as it suggests the surfaces are stable and are at a sufficient distance so as not collapse into one another.

It was found that no atoms had migrated across the grain boundary, suggesting that the surfaces were stable. There was some minor movement of atoms from their atomic sites at the grain boundary interface, which may have been due to the destibilising nature of the introduced surface.

6.3 Interaction between Palladium Hydride and Water

The relaxed palladium hydride grain boundary was used as a basis to study the interaction between palladium hydride and water. A well-established water model was used to describe the water molecules (de Leeuw and Parker 1998) although the potential was modified slightly in order to take account of the negative charge of the hydrogen atoms. To achieve this, the H-Ow A parameter was modified in line with the F-Ow interaction in fluorapetite ($Ca_{10}(PO_4)_6F_2$), (Mkhonto and de Leeuw 2002) as the hydrogen in palladium hydride is small and has a charge of -1, comparable to a fluorine atom. The parameters are outlined in Table 6-1.

Table 6-1: Parameters of an interatomic water potential describing the atomic interactions between palladium, hydrogen and water.

Interaction	Potential Type	A	ρ	C
Ow – Ow	Lennard-Jones	39344.98	42.15	-
Hw - Ow	9-6 Lennard-Jones	0.055	9	6
Pd - Ow	Buckingham	1925	0.215	0.00
H - Ow	Buckingham	79785221	0.120	26.788
H - Hw	Buckingham	715.3	0.25	0.00

795 water molecules were inserted into the simulation box around the palladium hydride grain boundary, along with 60 water molecules within the grain boundary gap itself in order to closely replicate the density of water. Initially, the hydrogen atoms were inserted in an ordered array, before being allowed to relax fully. Molecular Dynamics was then performed on the system, with an 40 ps equilibration of the system. Firstly, the NVE ensemble was used with the palladium hydride surface “frozen” and the temperature set to 0 K. This means that the palladium and hydrogen atoms were not permitted to move during the simulation. Next, NVT-hoover ensemble was performed with a “frozen” palladium hydride surface and at a temperature of 300 K. Finally, the palladium hydride surface was “unfrozen”, therefore allowing the palladium and hydrogen atoms to move freely using the NVT-hoover ensemble at 300 K.

A production run was then performed, consisting of 200 ps NPT-hoover. In total, 240 ps of simulation was carried out until the total energy of the system had converged and the water molecules had mixed well within the simulation box.

Figure 6-4 below shows snapshots of the palladium hydride – water system after 40 ps of equilibration. The snapshots were taken after 40, 60, 90, 140, 200 and 240 ps of the simulation, including 40 ps of equilibration and 200 ps of production.

As the simulation progresses, the water molecules become well mixed, filling all spaces within the simulation box. Additionally, the water molecules inside the grain boundary interact with the surface layer of the palladium hydride. Over time, the palladium hydride surface begins to rearrange to form a more planar outer surface, although some of the original structure can be identified, particularly close to the grain boundary. The grain boundary gap decreases as the two surface slabs begin to merge together and the inner water molecules effectively become trapped within the palladium hydride material. This behavior may be due to the grain boundary attempting to become more bulk-like, although the same behavior was not seen when the grain boundary did not include any water molecules. It should also be noted that no water molecules diffused into the material, although some interaction between the water and palladium hydride surface was observed.

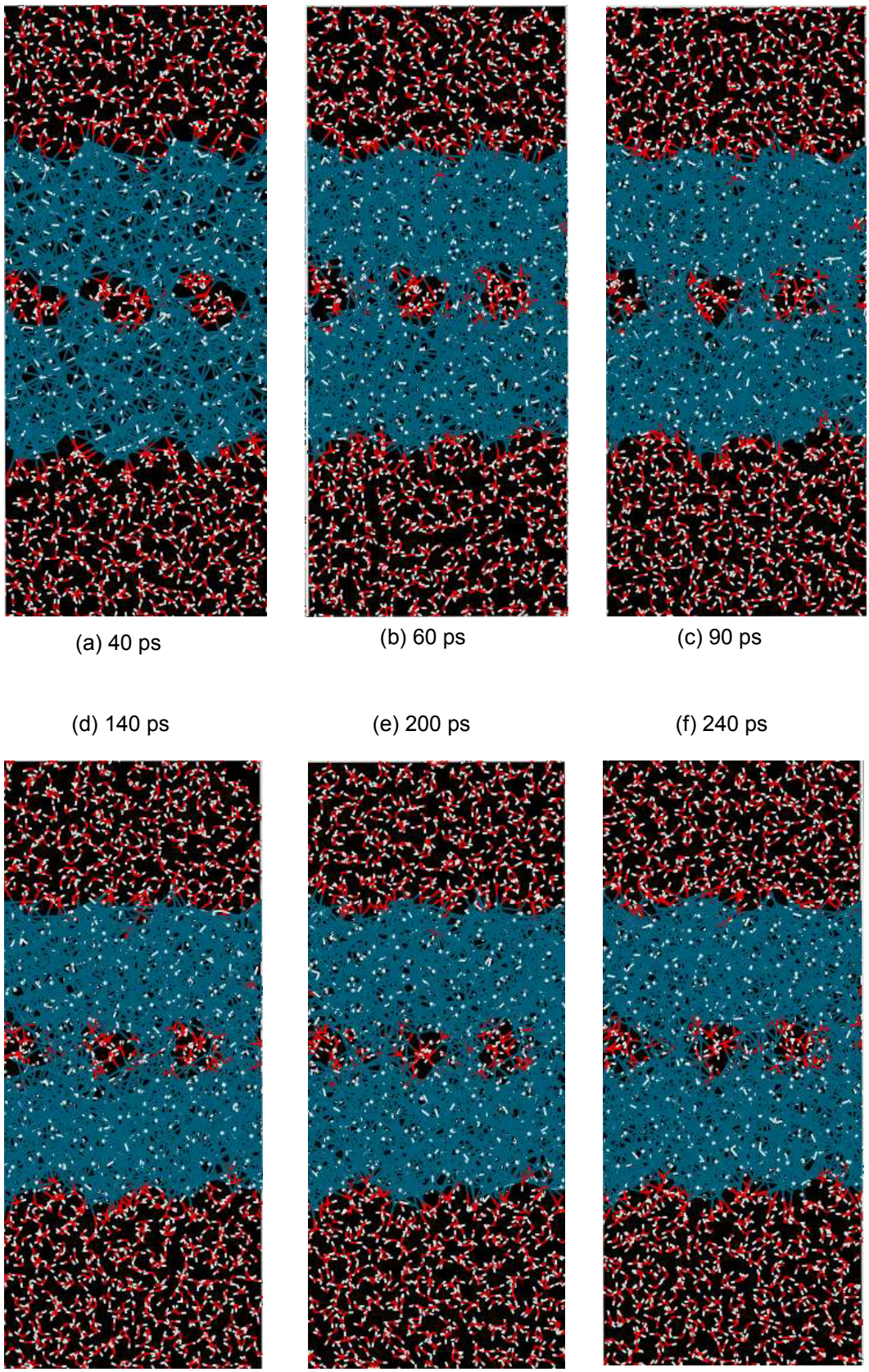

(a) 40 ps (b) 60 ps (c) 90 ps

(d) 140 ps (e) 200 ps (f) 240 ps

Figure 6-4: Snapshots of a palladium hydride grain boundary with 795 water molecules inserted into and around the grain boundary after: (a) 40 ps, (b) 60 ps, (c) 90 ps, (d) 140 ps, (e) 200 ps, (f) 240 ps of simulation.

Chapter 7

Discussion and Future Work

7.1 Discussion

A wide variety of computational techniques were presented in this work to study the properties of palladium hydride and palladium tritide. The use of different techniques has led to a well-rounded review of a number of properties.

A number of novel results have been presented in this work on palladium hydride including the use of Density Functional Theory to observe the distribution of hydrogen vacancies within the material, allowing the subsequent creation of a stable configuration of bulk $PdH_{0.75}$ and {100} $PdH_{0.75}$ surface. It was also possible to compare all common surfaces of PdH (namely {100}, {101} and {111} surfaces), whereas only the {111} PdH surface had previously been investigated in the literature. Finally, Molecular Dynamics was used to observe the interaction between a palladium hydride grain boundary and water molecules, which had not been studied previously in the literature.

Density Functional Theory was used to study the electronic properties of the material. Firstly, the Site Occupancy Disorder (SOD) code (Grau-Crespo et al. 2007) was used to explore the configurations created when a small number of hydrogen vacancies are introduced into palladium hydride. It was found that a large number of configurations are possible, although the number is greatly

reduced when considering symmetry operators and identical configurations are eliminated. Subsequently, DFT calculations were performed on each unique configuration and it was found that systems with vacancies spread throughout the material were more energetically stable than those with vacancies clustered together. This may be due to the destabilizing interaction experienced between two hydrogen vacancies as well as the ability to reduce the destabilizing effect as much as possible by spreading the vacancies throughout the material. This important finding was used as a foundation for all subsequent work on non-stoichiometric palladium hydride, as a means to easily understand which hydrogen atoms should be removed from the material to produce a stable system.

Other properties calculated using DFT included the effect of increasing tritium concentration, the proximity of helium to tritium atoms and helium migration. The activation energy of helium migration in $PdT_{0.9375}$, from one octahedral interstitial site to an adjacent octahedral site, in this work was found to be 1.419 eV. However, for the reverse direction the activation energy was found to be 1.423 eV. This may have been caused by the distribution of tritide atoms compared to the helium atom and octahedral interstitial vacancies. This work is comparable to Das et al. who calculated the activation energy between two octahedral interstitial sites as 1.05 or 1.14 eV (depending on direction of migration) within $PdT_{0.22}$ (Das et al. 2013). The difference in the two results can be attributed to the difference in palladium hydride/tritide formula. There are other studies(Zeng et al. 2006), (Xia et al. 2009) based on helium migration,

however these studies only consider the migration of helium in pure palladium metal so it is not possible to compare these results with this work.

These results provided a better understanding of the palladium tritide material including decay product helium-3. It was found that introduction of a helium atom into palladium metal has an effect on the lattice, that the total energy increases and the lattice shape becomes distorted. However, it was found that the distance between a tritium and helium atom had little effect on the total energy of the system or the cell dimensions.

Elastic constants and bulk modulus of palladium hydride were also calculated using DFT. These properties were vital in allowing the research to progress to interatomic potential development, as the Buckingham potential in this work was fitted to the DFT calculated properties.

The lattice parameter and elastic constants C_{11} and C_{44} of the palladium hydride interatomic potential derived in this work potential fitted well to DFT calculated values of PdH and experimental non-stoichiometric palladium hydride, with percentage errors between 0 and 4% *(Nygren and Leisure 1988)*. However, the C_{12} elastic constant did not fit well (with an error of 73.71 %) and as the bulk modulus depends on both C_{11} and C_{12}, this was also less accurate than hoped (28.33 %). The large percentage error was not expected and initially the reason for the discrepancy was not understood. In order to reduce the percentage error, a range of potential parameters were tested and an additional three-body hydrogen-palladium-hydrogen potential was investigated. However these methods did not reduce the percentage error and

time constraints meant that the percentage error could not be further improved. Despite the large inaccuracy of the fitted C_{12} elastic constant it was found that, particularly for palladium hydride, the interatomic potential was stable and accurately reproduced the structure and lattice constant of the material.

The large percentage error was due to the Cauchy relation, where $C_{12} = C_{44}$. However, palladium hydride violates the Cauchy relation and therefore $C_{12} \neq C_{44}$, as shown by elastic constants calculated by DFT in this work and experimental elastic constants (Nygren and Leisure 1988). When fitting the interatomic potentials, although $C_{12} \neq C_{44}$, it was not possible to obtain the large difference between C_{12} and C_{44} as observed for DFT and experimental values.

The violation of the Cauchy relation by palladium hydride was discovered after subsequent work had been completed on surfaces and grain boundaries using the derived Buckingham potential and time constraints meant that the work could not be redone. Future work should include the refinement of the Buckingham potential to take into account the Cauchy relation violation. In order to achieve this, a breathing shell model should be implemented within the GULP code (Gale 1997), rather than the rigid ion model or traditional core-shell model. The breathing shell model introduces an additional harmonic potential between the centre and the outer radius of the hydrogen shell, allowing for a change in the radius of the hydrogen atom. However, the simple rigid ion model used in this work is less computationally expensive and has led to interatomic potentials which model the surfaces of PdH well.

Four different surfaces of PdH and $PdH_{0.75}$; {100}, planar {101}, faceted {101} and {111} were analysed structurally and energetically. It is believed that this work is the first to study all surfaces of PdH and $PdH_{0.75}$ simultaneously. It was found that the {100} surface of PdH has the lowest total surface energy. For the three remaining surfaces, the $PdH_{0.75}$ surface is more energetically stable than the corresponding PdH surface, however greater distortion of atoms is found for the $PdH_{0.75}$ surfaces. The {111} surface for both PdH and $PdH_{0.75}$ is the least energetically stable and hence most reactive surface, which is expected as previous studies of reactions with palladium have focused on the {111} surface (Jigato et al. 2003). The inter-planar distances (i.e. the distance between surface layers) for each PdH surface converges to 0.001 Å after the 4^{th} layer and the inter-planar distance is larger for lower energy surfaces of PdH (i.e. the {100} surface). The {111} surface inter-planar distance in this work was found to converge to 0.001 Å after the 4^{th} surface layer, whereas the {111} surface inter-planar distances studied by Jigato *et al.* only converged to 0.1 Å after 13 surface layers, This suggests that the surface effects observed in this work do not influence the stability of the lower surface layers. Jigato et al. observed a large difference between the inter-planar distances of hydrogen-terminated and palladium-terminated {111} surfaces, whereas this work determined that the interplanar distances were very similar for both terminating variety of surface. Jigato *et al.* also suggested that the palladium-terminated {111} surface was less stable than the hydrogen-terminated surface, whereas this work found that both terminated surfaces had a similar total surface energy This work shows consistency in the inter-planar distances and of the properties

of palladium-terminated and hydrogen-terminated surfaces, suggesting that the interatomic potential is effective at modelling the PdH surface.

The distortion observed within the $PdH_{0.75}$ surfaces may have been due to the location of the hydrogen vacancies within the material. The studied configuration of each surface presented a low surface dipole compared to other “trial and error” configurations and therefore the chosen configurations were taken forward for energy minimisation and surface energy calculations. The Buckingham potential describing the $PdH_{0.75}$ system can be considered stable as bulk $PdH_{0.75}$ and $PdH_{0.75}$ {100} surface showed little distortion after relaxation. Further use of the Site Disorder Occupancy (SOD) code (Grau-Crespo et al. 2007) could allow a more stable configuration of $PdH_{0.75}$ to be identified, however a large number of energy minimisation calculations may still be required.

This work is the first in the literature to discuss the interaction of water with palladium hydride at the grain boundary, using Molecular Dynamics to model the system. It was found that the water molecules inside the grain boundary interacted with the surface layer of palladium hydride. As the simulation progressed the grain boundary gap decreased as the two surface slabs began to merge together and the inner water molecules effectively became trapped within the palladium hydride material. This behavior may be due to the grain boundary attempting to become more bulk-like, although the same behavior was not seen when the grain boundary did not include any water molecules. It should also be noted that after 240 ps, no diffusion of water molecules into the

material was observed, however there was some interaction between the water molecules and palladium hydride surface.

7.2 Future Work

Although helium-3 was studied in this work using Density Functional Theory, there is potential to explore the material further. As helium-3 is a decay product of tritium, helium atoms could be inserted into the grain boundary of palladium hydride created in this work to observe any atomic interactions. This would require the development of a helium – palladium and helium – hydrogen potential in order to carry out Molecular Dynamics simulations. The helium Density Functional Theory work in this thesis could be used as a benchmark to ensure the potential is fitted correctly. The fitting of the potential would present some challenges as the elastic constants of palladium tritide with helium have not been measured.

If a helium potential can be attained, there are a large number of properties which can be studied using Molecular Dynamics. As well as the aforementioned helium interaction with the palladium tritide grain boundary, helium atoms could be inserted into palladium tritide surfaces studied in this work at varying depths to investigate helium diffusion throughout the material and the mechanism for helium release from the surface. Helium clusters and bubbles could also be investigated further to study the mechanism of bubble formation, including whether smaller, adjacent clusters combine to form larger bubbles..

Ultimately, a large concentration of helium could be inserted in to palladium hydride to observe the mechanism of accelerated release. From this a critical concentration of helium could be calculated, leading to the estimation of a time length for the safe storage of tritium. This work could be completed initially with stoichiometric palladium tritide for simplicity before studying non-stoichiometric palladium tritide such as $PdT_{0.75}$.

Other future computational work could include the study of helium bubbles using DFT, by inserting a large number of helium atoms into a palladium tritide cell. This could provide insights into the energetics of helium bubbles, dependent on the number of helium atoms present. It would also be possible to observe the effect of the large helium bubble on surrounding atoms.

The stability of $PdH_{0.7}$ compared to other palladium hydride compositions is not currently explained within the literature. Future work could investigate this occurrence by exploring the different phases of palladium hydride and the relative stability of each phase. Further investigation of this phenomenon could include the study of the density of states of palladium hydride and studying palladium hydride at increasingly high pressures in order to achieve stoichiometric PdH.

Results from this body of work and any future work could be used to complement experimental studies. This could include using the surfaces studied in this work to experimentally investigate the stability of each surface and the behaviour of surface atoms. This could then be further developed to

include the study of the lifetime of tritium storage within palladium metal and the occurrence of surface defects due to helium bubble formation and release.

References

Abell, G. C., Matson, L.K., Steinmeyer, R.H., Bowman, R.C. and Oliver, B.M. (1990). "Helium Release From Aged Palladium Tritide." Physical Review B **41**(2): 1220-1223.

Ackland, G. J., Tichy, G., Vitek, V. and Finnis, M.W. (1987). "Simple N-Body Potentials For The Noble-Metals And Nickel." Philosophical Magazine a-Physics of Condensed Matter Structure Defects and Mechanical Properties **56**(6): 735-756.

Adams, B. D. and Chen A. (2011). "The role of palladium in a hydrogen economy." Materials Today **14**(6): 282-289.

Andersen, O. K. (1975). "Linear Methods In Band Theory." Physical Review B **12**(8): 3060-3083.

Baskes, M. I. and Melius, C.F. (1979). "Pair Potentials For Fcc Metals." Physical Review B **20**(8): 3197-3204.

Beavis, L. C. and Kass, W.J. (1977). "Room-Temperature Desorption Of He-3 From Metal Tritides - Tritium Concentration Effect On Rapid Release Of Helium From Tritide." Journal of Vacuum Science & Technology **14**(1): 509-513.

Beavis, L. C. and Miglioni, C.J. (1972). "Structural Behavior Of Metal Tritide Films." Journal of the Less-Common Metals **27**(2): 201-&.

Beck, D. E. (1968). "A New Interatomic Potential Function For Helium." Molecular Physics **14**(4): 311-&.

Berube, V., Radtke, G., Dresselhaus, M. and Chen, G. (2007). "Size effects on the hydrogen storage properties of nanostructured metal hydrides: A review." International Journal of Energy Research **31**(6-7): 637-663.

Boys, S. F. (1950). "Electronic wave functions. I. A general method of calculation for the stationary states of any molecular system". Proceedings of the Royal Society of London Series A-Mathematical and Physical Sciences **200**(1063):542–554.

Briec, M., Botter, F., Abassin, J.J., Benoit, R., Chenebault, P., Masson, M., Rasneur, B., Sciers, P., Werle, H. and Roth, E. (1986). "In And Out-Of-Pile Tritium Extraction From Samples Of Lithium Aluminates." Journal of Nuclear Materials **141**: 357-363.

Buckingham, R. A. (1938). "The classical equation of state of gaseous helium, neon and argon." Proceedings of the Royal Society of London Series a-Mathematical and Physical Sciences **168**(A933): 264-283.

Camp, W. J. (1977). "Helium Detrapping And Release From Metal Tritides." Journal of Vacuum Science & Technology **14**(1): 514-517.

Clark, E. (2004). "Estimate Of Tritium Permeation Out Of Tpbar Waste Container (U)"**:** US Department of Energy WSRC-T-2004-00424

Cowgill, D. F. (2004). "Helium nano-bubble evolution in aging metal tritides" Sandia National Laboratories SAND2004-1739 C.2

Das, N. K., Rigby, K. and de Leeuw, N. H. (2014). "The effect of helium nano-bubbles on the structures stability and electronic properties of palladium tritides: a density functional theory study." Proceedings of the Royal Society a-Mathematical Physical and Engineering Sciences **470**(2171).

Daw, M. S. and Baskes, M. I. (1983). "Semiempirical, Quantum-Mechanical Calculation Of Hydrogen Embrittlement In Metals." Physical Review Letters **50**(17): 1285-1288.

de Leeuw, N. H. and Parker, S.C. (1998). "Molecular-dynamics simulation of MgO surfaces in liquid water using a shell-model potential for water." Physical Review B **58**(20): 13901-13908.

Emig, J. A., Garza R., Christensen, L.D., Coronado, P.R. and Souers, P.C. (1992). "Helium Release From 19-Year-Old Palladium Tritide." Journal of Nuclear Materials **187**(3): 209-214.

Flanagan, T. B. and Oates, W.A. (1991). "The Palladium-Hydrogen System." Annual Review of Materials Science **21**: 269-304.

Fukai, Y. and Okuma, N. (1994). "[Of Superabundant Vacancies In Pd Hydride Under High Hydrogen Pressures." Physical Review Letters **73**(12): 1640-1643.

Gale, J. D. (1997). "GULP: A computer program for the symmetry-adapted simulation of solids." Journal of the Chemical Society-Faraday Transactions **93**(4): 629-637.

Gillan, M. J. (1986). "A Simulation-Model For Hydrogen In Palladium .1. Single-Particle Dynamics." Journal of Physics C-Solid State Physics **19**(31): 6169-6184.

Grau-Crespo, R., Hamad, S., Catlow, C. R. A. and de Leeuw, N.H. (2007). "Symmetry-adapted configurational modelling of fractional site occupancy in solids." Journal of Physics-Condensed Matter **19**(25).

Gupta, M. (2000). "Electronic structure of hydrogen storage materials." International Journal of Quantum Chemistry **77**(6): 982-990.

Gupta, R. P. and Gupta, M. (2002). "Consequences of helium production from the radioactive decay of tritium on the properties of palladium tritide." Physical Review B **66**(1): 4.

Haque, E. and Islam, A. (1992). "Hydrides And Deuterides Of Lithium And Sodium - Model Potentials And Their Use In Defect Lattice." Journal of Physics and Chemistry of Solids **53**(3): 377-382.

Hemmes, H., Driessen, A., Griessen, R. and Gupta, M. (1989). "Isotope Effects And Pressure-Dependence Of The Tc Of Superconducting Stoichiometric Pdh And Pdd Synthesized And Measured In A Diamond Anvil Cell." Physical Review B **39**(7): 4110-4118.

Holder, J. S. and Wermer, J.R. (1995). "Thermodynamic characterization of new palladium alloy tritides." Journal of Alloys and Compounds **231**(1-2): 773-779.

Hoover, W. G. (1985). "Canonical Dynamics - Equilibrium Phase-Space Distributions." Physical Review A **31**(3): 1695-1697

Jigato, M. P., Coussens, B. and King, D.A. (2003). "The crystalline surfaces of beta-PdH{111}: Ideal surface terminations of a stoichiometric bulk compound relevant to heterogeneous catalysis." Journal of Chemical Physics **118**(12): 5623-5634.

Johnson, R. A. (1973). "Empirical Potentials And Their Use In Calculation Of Energies Of Point-Defects In Metals." Journal of Physics F-Metal Physics **3**(2): 295-321.

Joubert, J. M. and Thiebaut, S. (2009). "Thermodynamic assessment of the Pd-H-D-T system." Journal of Nuclear Materials **395**(1-3): 79-88.

Kamakoti, P. and Sholl, D. S. (2003). "A comparison of hydrogen diffusivities in Pd and CuPd alloys using density functional theory." Journal of Membrane Science **225**(1-2): 145-154.

Kohn, W. and Sham, L. J. (1965). "Self-Consistent Equations Including Exchange And Correlation Effects." Physical Review **140**(4A): 1133-&.

Kresse, G. and Furthmuller, J. (1996). "Efficiency of ab-initio total energy calculations for metals and semiconductors using a plane-wave basis set." Computational Materials Science **6**(1): 15-50.

Kresse, G. and Furthmuller, J. (1996). "Efficient iterative schemes for ab initio total-energy calculations using a plane-wave basis set." Physical Review B **54**(16): 11169-11186.

Kresse, G. and Hafner, J. (1993). "Abinitio molecular-dynamics for liquid-metals." Physical Review B **47**(1): 558-561.

Kresse, G. and Hafner, J. (1994). "Ab-Initio Molecular-Dynamics Simulation Of The Liquid-Metal Amorphous-Semiconductor Transition In Germanium." Physical Review B **49**(20): 14251-14269.

Lasser, R. (1987). "Properties Of Tritium And He-3 In Metals." Journal of the Less-Common Metals **131**: 263-273.

Leach, A. R. (2001). Molecular Modelling: Principles and Applications, Prentice Hall.

Liu, T. J., Wang, Y. X., Pan, Z. Y., Jiang, X. M., Zhou, L. and Zhu, J. (2006). "Atomistic simulation of He clustering and defects produced in Ni." Chinese Physics Letters **23**(5): 1261-1264.

Maeland, A. and Flanagan, T. (1966). "The Hydrogen-Palladium System." Platinum Metals Rev **10**(1): 20-23.

Maeland, A. and Flanagan, T. B. (1964). "Lattice Constants + Thermodynamic Parameters Of Hydrogen-Platinum-Palladium + Deuterium-Platinum-Palladium Systems." Journal of Physical Chemistry **68**(6): 1419-&.

Melius, C. F., Bisson, C. L. and Wilson, W.D. (1978). "Quantum-Chemical And Lattice-Defect Hybrid Approach To Calculation Of Defects In Metals." Physical Review B **18**(4): 1647-1657.

Mitchell, D. J. and Provo, J. L. (1985). "Irregularities In Helium Release Rates From Metal Ditritides." Journal of Applied Physics **57**(6): 1855-1860.

Mkhonto, D. and de Leeuw, N. H. (2002). "A computer modelling study of the effect of water on the surface structure and morphology of fluorapatite: introducing a Ca-10(PO4)(6)F-2 potential model." Journal of Materials Chemistry **12**(9): 2633-2642.

Monkhorst, H. J. and Pack, J. D. (1976). "Special points for Brillouin-zone integrations". Physical Review B **13**(12): 5188–5192.

Moriyama, H., Tanaka, S., Sze, D. K., Reimann, J. and Terlain, A. (1995). "Tritium Recovery From Liquid-Metals." Fusion Engineering and Design **28**: 226-239.

Myers, S. M., Richards, P. M., Follstaedt, D. M. and Schirber, J. E. (1991). "Superstoichiometry, Accelerated Diffusion, And Nuclear-Reactions In Deuterium-Implanted Palladium." Physical Review B **43**(12): 9503-9510.

Nolan, S. J., Gillan, M. J., Alfe, D., Allan, N. L. and Manby, F. R. (2009). "Calculation of properties of crystalline lithium hydride using correlated wave function theory." Physical Review B 80 (16):165109

Nygren, L. A. and Leisure, R. G. (1988). "Elastic-Constants Of Alpha'-Phase Pdhx Over The Temperature-Range 4-300 K." Physical Review B **37**(11): 6482-6485.

Okuyama, H., Siga, W., Takagi, N., Nishijima, M. and Aruga, T. (1998). "Path and mechanism of hydrogen absorption at Pd(100)." Surface Science **401**(3): 344-354.

Orimo, S. and Fujii, H. (2001). "Materials science of Mg-Ni-based new hydrides." Applied Physics a-Materials Science & Processing **72**(2): 167-186.

Ovshinsky, S. R., Fetcenko, M. A. and Ross, J. (1993). "A Nickel Metal Hydride Battery For Electric Vehicles." Science **260**(5105): 176-181.

Pandey, R. and Stoneham, A. M. (1985). "Intrinsic Defect Energies Of Lithium Hydride And Lithium Deuteride Crystals." Journal of Physics C-Solid State Physics **18**(27): 5289-5297.

Perdew, J. P., Chevary, J. A., Vosko, S. H., Jackson, K. A., Pederson, M. R., Singh, D. J. and Fiolhais, C. (1992). "Atoms, Molecules, Solids, And Surfaces - Applications Of The Generalized Gradient Approximation For Exchange And Correlation." Physical Review B **46**(11): 6671-6687.

Perdew, J. P., Chevary, J. A., Vosko, S. H., Jackson, K. A., Pederson, M. R., Singh, D. J. and Fiolhais, C. (1993). "Atoms, Molecules, Solids, And Surfaces

- Applications Of The Generalized Gradient Approximation For Exchange And Correlation (VOL 46, PG 6671, 1992)." Physical Review B **48**(7): 4978-4978.

Pratt, L. R. and Eckert, J. (1989). "Molecular-Dynamics Of A Dilute-Solution Of Hydrogen In Palladium." Physical Review B **39**(18): 13170-13174.

Robinson, D. B., Fares, S. J., Ong, M. D., Arslan, I., Langham, M. E., Tran, K. L. and Clift, W. M. (2009). "Scalable synthesis of nanoporous palladium powders." International Journal of Hydrogen Energy **34**(13): 5585-5591.

Ruda, M., Crespo, E. A. and Ramos de Debiaggi, S. (2010). "Atomistic modeling of H absorption in Pd nanoparticles." Journal of Alloys and Compounds **495**(2): 471-475.

Schlapbach, L. and Zuttel, A. (2001). "Hydrogen-storage materials for mobile applications." Nature **414**(6861): 353-358.

Schwarz, R. B., Bach, H. T., Harms, U.and Tuggle, D. (2005). "Elastic properties of Pd-hydrogen, Pd-deuterium, and Pd-tritium single crystals." Acta Materialia **53**(3): 569-580.

Slater, J. C. (1930). "Atomic shielding constants". Physical Review **36**(1):0057–0064.

Stritzke.B and Buckel, W. (1972). "Superconductivity In Palladium-Hydrogen And Palladium-Deuterium Systems." Zeitschrift Fur Physik **257**(1): 1-8.

Thiebaut, S., Douilly, M., Contreras, S., Limacher, B., Paul-Boncour, V., Decamps, B. and Percheron-Guegan A. (2007). "He-3 retention in LaNi5 and Pd tritides: Dependence on stoichiometry, He-3 distribution and aging effects." Journal of Alloys and Compounds **446**: 660-669.

Thiebaut, S., Paul-Boncour, V., Percheron-Guegan, A., Limacher, B., Blaschko, O., Maier, C., Tailland, C. and Leroy, D. (1998). "Structural changes in Pd (Rh, Pt) solid solutions due to He-3 formation during tritium storage." Physical Review B **57**(17): 10379-10387.

Verlet, L. (1967). "Computer Experiments On Classical Fluids .I. Thermodynamical Properties Of Lennard-Jones Molecules." Physical Review **159**(1): 98-&.

Wang, L., Hu, W., Xiao, S., Yang, J. and Deng, H. (2009). "Atomistic simulation of helium bubble nucleation in palladium." Nuclear Instruments & Methods in Physics Research Section B-Beam Interactions with Materials and Atoms **267**(18): 3185-3188.

Watson, G. W., Kelsey, E. T., de Leeuw, N. H., Harris, D. J. and Parker, S. C. (1996). "Atomistic simulation of dislocations, surfaces and interfaces in MgO." Journal of the Chemical Society-Faraday Transactions **92**(3): 433-438.

Wilson, W. D. (1983). "Theory Of Small Clusters Of Helium In Metals." Radiation Effects and Defects in Solids **78**(1-4): 11-24.

Worsham, J. E., Wilkinson, M. K. and Shull, C. G. (1957). "Neutron-Diffraction Observations On The Palladium-Hydrogen And Palladium-Deuterium Systems." Journal of Physics and Chemistry of Solids **3**(3-4): 303-310.

Xia, J. X., Hu, W. Y., Yang, T. Y., Ao, B. Y. and Wang, X. L. (2006). "A comparative study of helium atom diffusion via an interstitial mechanism in nickel and palladium." Physica Status Solidi B-Basic Solid State Physics **243**(3): 579-583.

Yang, J. Y., Hu, W. Y., Deng, H. Q. and Zhao, D. L. (2004). "Temperature dependence of atomic relaxation and vibrations for the vicinal Ni(977) surface: a molecular dynamics study." Surface Science **572**(2-3): 439-448.

Zeng, X., et al. (2009). "First-principles approach to the properties of point defects and small helium-vacancy clusters in palladium." Nuclear Instruments & Methods in Physics Research Section B-Beam Interactions with Materials and Atoms **267**(18): 3037-3040.

Zheng, H., Liu, S., Yu, H. B., Wang, L. B., Liu, C. Z. and Shi, L. Q. (2005). "Introduction of helium into metals by magnetron sputtering deposition method." Materials Letters **59**(8-9): 1071-1075.

Zhou, X. W., Zimmerman, J. A., Wong, B. M. and Hoyt, J. J. (2008). "An embedded-atom method interatomic potential for Pd-H alloys." Journal of Materials Research **23**(3): 704-718.

Zhu, H.-Z., Zhu, X.-L. and Wei, Y.-J. (2008). "Kinetic properties during absorption in aged palladium-tritium system." Journal of Alloys and Compounds **461**(1-2): 285-291.

Zimmerman, J. A., Hoyt, J. J., Leonard, F. L., Griffin, J. D. and Xiao, W. (2007). Development of an inter-atomic potential for the Pd-H binary system**:** Medium: ED; Size: 198 p.

Zu, X. T., Yang, L., Gao, F., Peng, S. M., Heinisch, H. L., Long, X. G. and Kurtz, R. J. (2009). "Properties of helium defects in bcc and fcc metals investigated with density functional theory." Physical Review B **80**(5): 6.